NATIONAL ADVISORY COMMITTEE FOR AERONAUTICS

TECHNICAL NOTE 4148

THEORETICAL PRESSURE DISTRIBUTIONS FOR SEVERAL RELATED NONLIFTING AIRFOILS AT HIGH SUBSONIC SPEEDS

By John R. Spreiter, Alberta Y. Alksne,
and B. Jeanne Hyett

Ames Aeronautical Laboratory
Moffett Field, Calif.

Washington

January 1958

L

TABLE OF CONTENTS

NATIONAL ADVISORY COMMITTEE FOR AERONAUTICS

TECHNICAL NOTE 4148

THEORETICAL PRESSURE DISTRIBUTIONS FOR SEVERAL RELATED NONLIFTING AIRFOILS AT HIGH SUBSONIC SPEEDS

By John R. Spreiter, Alberta Y. Alksne,
and B. Jeanne Hyett

SUMMARY

Theoretical pressure distributions on five related airfoils, including thin symmetrical circular-arc airfoils, in two-dimensional flows with high subsonic free-stream velocity are presented. The airfoils have various locations for the point of maximum thickness ranging from 30- to 70-percent chord and are of arbitrary, although small, thickness ratio. The results are obtained by approximate solution, through an iteration process, of a nonlinear integral equation derived from the equations of transonic flow theory. It is shown that the pressure distributions display most of the principal phenomena observed in experimental studies, and are in good correspondence with those calculated by other methods for subcritical Mach numbers and for Mach numbers near 1.

INTRODUCTION

The equations governing transonic flows are known and well established by favorable comparisons with experiment. Although the difficulties arising as a result of the nonlinearity and mixed character of the differential equation for the potential have hindered the advancement of the analysis, approximate methods are gradually emerging that permit the theoretical prediction of pressure distributions on a wide variety of shapes of aerodynamic interest.

One of these methods is that described in reference 1 in which the differential equation of transonic flow theory is recast into the form of a nonlinear integral equation and approximate solutions are sought by application of an iteration procedure. The iteration procedure is of the successive approximation type, but differs from the related procedures customarily employed to determine higher approximations to the solutions of problems of compressible flow theory in that the quadratic nature of the integral equation is recognized and retained throughout the analysis. This method is described in general in reference 1 and is applied to a nonlifting symmetrical circular-arc airfoil for which pressure distributions are calculated for a range of Mach numbers extending from well below the critical Mach number up to unity. The results indicate most of the principal phenomena observed in experimental studies. Certain aspects of

the results for free-stream Mach numbers near unity are not as satisfactory as for lower, but still supercritical, Mach numbers, however, and it is now evident that one of the simplifying approximations needs refinement before results of good quality can be calculated for flows in which the free-stream Mach number approaches unity.

Although it would be interesting and worthwhile to develop the necessary refinement to extend the Mach number range over which the method of reference 1 can be applied satisfactorily, the need for such a refinement has been greatly reduced by the development of a second approximate method described in reference 2. The latter method enables the determination of expressions in closed analytic form for the pressure distributions on a wide variety of airfoils in flows with free-stream Mach numbers equal to or near unity. A large number of specific results are given in reference 2, but particular attention is focused on a family of airfoils, including symmetrical circular-arc airfoils, that have the point of maximum thickness located at 30-, 40-, 50-, 60-, and 70-percent chord, and for which experimental pressure distributions are available from references 3 and 4. These results indicate pronounced effects of airfoil shape, but provide no information on the transition from the pressure distributions of subsonic type that occur at all Mach numbers below the critical to the pressure distributions of sonic type that occur at free-stream Mach numbers near unity. Theoretical pressure distributions can be calculated for most of the intervening Mach number range by application of the method of reference 1, however, and it is the principal purpose of this paper to present and discuss the results of such calculations for the particular family of airfoils referred to above. A resumé of the method of reference 1 precedes the presentation of the results.

PRINCIPAL SYMBOLS

b function defined in equation (20)

C_p pressure coefficient, $\dfrac{p-p_\infty}{\frac{\rho_\infty}{2} U_\infty^2}$

$\overline{C}_p$ $\dfrac{(U_\infty k)^{1/3}}{\tau^{2/3}} C_p$

c chord

c_d section pressure drag coefficient, $\dfrac{d}{\frac{\rho_\infty}{2} U_\infty^2 c}$

$\overline{c}_d$ $\dfrac{(U_\infty k)^{1/3}}{\tau^{5/3}} c_d$

d	pressure drag
E	function defined in equation (22)
f	function defined in equations (24) and (25)
H	$\frac{h}{c}$
$\overline{H}$	$H(U_\infty k_T)^{1/3}$
h	half height of wind tunnel
I	function defined in equation (16)
k	$\frac{M_\infty^2(\gamma+1)}{U_\infty}$
L	$2\overline{u}_L - 1$
l	width of element used in approximating the chordwise velocity distribution
M	local Mach number
M_{cr}	critical Mach number
M_∞	free-stream Mach number
p	static pressure
p_∞	free-stream static pressure
r_2	$\sqrt{(\overline{x}-\overline{\xi})^2 + (\overline{z}-\overline{\zeta})^2}$
t	maximum thickness of profile
U_∞	free-stream velocity
u,w	perturbation velocity components parallel to the x,z axes, respectively
$\overline{u}$	$\frac{k}{\beta^2} u$
$\overline{w}$	$\frac{k}{\beta^3} w$
x,z	Cartesian coordinates

$\overline{x}$ x

$\overline{z}$ βz

Z ordinates of wing profiles

$\overline{Z}$ $\frac{kU_\infty}{\beta^3} Z$

β $\sqrt{1-M_\infty^2}$

γ ratio of specific heats, 1.4 for air

$\Delta\overline{C}_p$ $\overline{C}_p - \overline{C}_{p_{WT}}$

$\Delta\xi_\infty$ $\xi_\infty - \xi_{\infty_{WT}}$

$\overline{\xi},\overline{\zeta}$ variables of integration corresponding to $\overline{x},\overline{z}$

ξ $-\frac{1-M^2}{(U_\infty k\tau)^{2/3}}$

ξ_∞ $-\frac{1-M_\infty^2}{(U_\infty k\tau)^{2/3}}$

ρ_∞ free-stream density of air

τ $\frac{t}{c}$

$\overline{\tau}$ $\frac{kU_\infty}{\beta^3} \tau$

φ perturbation velocity potential

$\overline{\varphi}$ $\frac{k}{\beta^2} \varphi$

Subscripts

a values ahead of shock wave

b values behind shock wave

cr conditions associated with the critical Mach number

L values given by linear compressible-flow theory

W values at the wing surface

WT wind tunnel

Superscript

* values associated with the sonic point

DESCRIPTION OF AIRFOILS

The airfoils considered in this paper are exactly those for which experimental data are given by Michel, Marchaud, and Le Gallo in references 3 and 4. The ordinates Z of the airfoils that have the point of maximum thickness at 60- and 70-percent chord are given by

$$\frac{Z}{c} = A\left[\frac{x}{c} - \left(\frac{x}{c}\right)^n\right] \tag{1}$$

where n has the values 3.38 and 6.05, respectively, and A is related to the thickness ratio τ by

$$A = \frac{n^{n/(n-1)}}{2(n-1)}\tau \tag{2}$$

The ordinates of the airfoils that have the point of maximum thickness at 30- and 40-percent chord are given by

$$\frac{Z}{c} = A\left[\left(1 - \frac{x}{c}\right) - \left(1 - \frac{x}{c}\right)^n\right] \tag{3}$$

where n has the values 6.05 and 3.38, respectively, and A is related to the thickness ratio by equation (2). The ordinates of the airfoils that have the point of maximum thickness at 50-percent chord are special cases of either of the families of airfoils defined by equation (1) or (3) when n is equated to 2, and are the same as those of the airfoils for which theoretical results are given in reference 1. The latter

airfoils may be referred to as either parabolic-arc or circular-arc airfoils since the two classes of shapes are indistinguishable to the order of accuracy of the small-disturbance theory of transonic flow.

RESUMÉ OF THEORY

The new results presented in this paper are determined by direct application of the method of reference 1 to the specific airfoils described in the preceding section. A resumé of the parts of reference 1 that pertain specifically to the determination of pressure distributions on symmetrical nonlifting airfoils is given here in the interest of completeness, and in order to provide an opportunity for additional comments on certain points beyond those provided originally in reference 1.

Fundamental Equations and Boundary Conditions

Consider the steady flow of an inviscid compressible gas past an arbitrary symmetrical nonlifting airfoil of chord c and thickness ratio τ. Introduce Cartesian coordinates x and z with the x axis parallel to the direction of the free stream as illustrated in sketch (a). Let the free-stream velocity and density be U_∞ and ρ_∞, the perturbation potential be φ, and the perturbation velocity components parallel to the x and z axes be φ_x, or u, and φ_z, or w, where the subscript indicates differentiation. The boundary conditions require that the perturbation velocities vanish at infinity, and that the flow is tangential to the wing surface. The former condition indicates that φ is a constant at infinity. The latter condition can be approximated for thin wings by

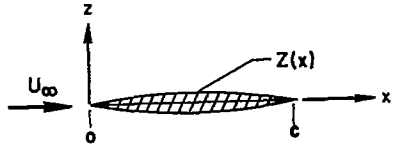

Sketch (a)

$$(\varphi_z)_{z=0} = U_\infty \frac{dZ}{dx} \tag{4}$$

where Z represents the ordinates of the airfoil upper surface. The differential equation for φ in the small-disturbance theory of transonic flow is

$$(1-M_\infty^2)\varphi_{xx}+\varphi_{zz} = M_\infty^2 \frac{\gamma+1}{U_\infty} \varphi_x\varphi_{xx} = k\varphi_x\varphi_{xx} \tag{5}$$

where M_∞ is the Mach number of the undisturbed flow and γ is the ratio of specific heats (1.4 for air).

Equation (5) is, of course, valid only in regions where the necessary derivatives exist and are continuous. Since these conditions do not hold where shock waves occur, and since shock waves are a prominent feature of most transonic flows, an additional equation is needed for the transition through the shock. The fundamental properties of a shock surface require that the normal component of velocity be discontinuous and the tangential component, and therefore φ, be continuous. The necessary relation follows from the classical expression for the shock polar which, in the small-disturbance transonic theory, is approximated by

$$(1-M_\infty^2)(u_a-u_b)^2+(w_a-w_b)^2 = M_\infty^2 \frac{\gamma+1}{U_\infty} \frac{u_a+u_b}{2} (u_a-u_b)^2 \tag{6}$$

where the subscripts a and b refer to conditions ahead of and behind the shock.

Upon solving the above boundary-value problem for the perturbation potential, one may determine the pressure coefficient by means of the approximate relation

$$C_p = \frac{p-p_\infty}{\frac{\rho_\infty}{2} U_\infty^2} = -\frac{2}{U_\infty} \frac{\partial \varphi}{\partial x} \tag{7}$$

An important quantity in the discussion of compressible flows is the critical pressure coefficient $C_{p_{cr}}$ associated with the local occurrence of sonic velocity. The appropriate relation is found by combination of equation (7) and the expression obtained by equating to zero the total coefficient of φ_{xx} in equation (5), and is

$$C_{p_{cr}} = -\frac{2(1-M_\infty^2)}{M_\infty^2(\gamma+1)} \tag{8}$$

The analysis presented in reference 1 is based upon consideration of the preceding equations recast into a normalized form by introduction of reduced variables. The definitions of these quantities, together with additional useful relations, are given below.

$$\bar{x} = x \qquad \bar{z} = \beta z \qquad \bar{\varphi} = \frac{k}{\beta^2}\varphi$$

$$\bar{Z} = \frac{kU_\infty}{\beta^3} Z \qquad \bar{u} = \frac{\partial\bar{\varphi}}{\partial\bar{x}} = \frac{k}{\beta^2} u \qquad \bar{w} = \frac{\partial\bar{\varphi}}{\partial\bar{z}} = \frac{k}{\beta^3} w$$

$$\bar{C}_p = \frac{(U_\infty k)^{1/3}}{\tau^{2/3}} C_p \qquad \xi_\infty = \frac{-\beta^2}{(U_\infty k\tau)^{2/3}} \qquad \xi = -\frac{1-M^2}{(U_\infty k\tau)^{2/3}}$$

$$\bar{\tau} = \frac{kU_\infty}{\beta^3}\tau \qquad \xi_\infty = -\frac{1}{\bar{\tau}^{2/3}} \qquad \xi = \frac{\bar{u}-1}{\bar{\tau}^{2/3}}$$

$$\bar{C}_p = -2\frac{\bar{u}}{\bar{\tau}^{2/3}} = -2(\xi-\xi_\infty) \qquad \bar{C}_{p_{cr}} = 2\xi_\infty$$

where

$$\beta = \sqrt{1-M_\infty^2} \qquad k = \frac{M_\infty^2(\gamma+1)}{U_\infty} \tag{9}$$

In this way, the differential equation given by equation (5) reduces to

$$\bar{\varphi}_{\bar{x}\bar{x}} + \bar{\varphi}_{\bar{z}\bar{z}} = \bar{\varphi}_{\bar{x}}\bar{\varphi}_{\bar{x}\bar{x}} \tag{10}$$

or to

$$(1-\bar{u})\bar{\varphi}_{\bar{x}\bar{x}} + \bar{\varphi}_{\bar{z}\bar{z}} = 0 \tag{11}$$

It is apparent from equation (11) that $\bar{u} < 1$ when the local velocity is subsonic, $\bar{u} = 1$ when it is sonic, and $\bar{u} > 1$ when it is supersonic. Similarly, the expression for the shock relation given by equation (6) reduces to

$$(\bar{u}_a-\bar{u}_b)^2+(\bar{w}_a-\bar{w}_b)^2=\left(\frac{\bar{u}_a+\bar{u}_b}{2}\right)(\bar{u}_a-\bar{u}_b)^2 \tag{12}$$

If the shock wave is a normal wave and the flow is parallel to the $\bar{x}$ axis (i.e., $\bar{w}_a = \bar{w}_b = 0$, but $\bar{u}_a \neq \bar{u}_b$), it can be seen from equation (12) that the reduced perturbation velocity component $\bar{u}$ jumps from $1 + \Delta$ immediately ahead of the shock to $1 - \Delta$ immediately behind the shock. The quantity $\bar{u}-(\bar{u}^2/2)$, on the other hand, is equal on the two sides of the shock. The latter result is consistent with the fact that the quantity $\bar{u}-(\bar{u}^2/2)$ corresponds, in the transonic approximation, to the mass flow, which is continuous through a normal shock.

An Integral Equation for Transonic Flow

Approximate solutions for the pressure distribution on symmetrical nonlifting airfoils in mixed or transonic flows are sought in the method of reference 1 by consideration of the following integral equation derived from the differential equations given in the preceding section by application of Green's theorem:

$$\bar{u}(\bar{x},\bar{z}) = \bar{u}_L(\bar{x},\bar{z}) + \frac{\bar{u}^2(\bar{x},\bar{z})}{2} - \frac{1}{2\pi}\int_{-\infty}^{+\infty}\iint \frac{\bar{u}^2}{2}\frac{\partial^2}{\partial\bar{\xi}^2}\ln\left(\frac{1}{r_2}\right)d\bar{\xi}\,d\bar{\zeta} \tag{13}$$

where

$$r_2 = \sqrt{(\bar{x}-\bar{\xi})^2+(\bar{z}-\bar{\zeta})^2}$$

The term $\bar{u}_L$ that appears in equation (13) represents the values for $\bar{u}$ given by linearized compressible flow theory. Its values can be obtained by application of the following well-known expression:

$$\bar{u}_L = -\frac{1}{\pi}\frac{\partial}{\partial\bar{x}}\int_0^c \frac{d\bar{Z}}{d\bar{\xi}}\ln\frac{1}{\sqrt{(\bar{x}-\bar{\xi})^2+\bar{z}^2}}\,d\bar{\xi} \tag{14}$$

The derivation of equation (13), presented in reference 1, requires the introduction of two slightly contradictory statements regarding the nature of the shock waves. They are: (a) All shock waves are assumed to lie in a plane perpendicular to the x axis, and (b) the shock waves are assumed to be normal shock waves (i.e., normal to the local flow direction). A new derivation of equation (13) has been given subsequently

in reference 5, however, in which it is shown that it is not necessary to introduce these two assumptions, and that this integral equation is, indeed, an exact relation within the framework of transonic small-disturbance theory.

It is helpful to consider, before proceeding to the details of the approximate solution of equation (13), a summary of the discussion given in reference 1 concerning some properties of the nonlinear integral equation and of its solution. The first and simplest property is that the solutions of equation (13) must approach those of linear theory when the free-stream Mach number is much less than the critical Mach number, since $\bar{u} \ll 1$ and the terms involving the square of $\bar{u}$ become negligible with respect to those linear in $\bar{u}$, thereby leaving only

$$(\bar{u})_{M_\infty \ll 1} \approx \bar{u}_L \tag{15}$$

Further discussion of the properties of equation (13) is facilitated by introduction of the abbreviation $I/2$ for the integral, so that

$$\bar{u} = \bar{u}_L + \frac{\bar{u}^2}{2} - \frac{I}{2} \tag{16}$$

where

$$I = 2\left[\frac{1}{2\pi}\int_{-\infty}^{+\infty}\int \frac{\bar{u}^2}{2}\frac{\partial^2}{\partial\bar{\xi}^2}\ln\left(\frac{1}{r_2}\right)d\bar{\xi}\,d\bar{\zeta}\right]$$

Although I is a function of $\bar{u}$ and is therefore unknown, it is informative to rewrite equation (13) by solving for $\bar{u}$ in terms of I and $\bar{u}_L$, thus

$$\bar{u} = 1 \pm \sqrt{I-(2\bar{u}_L-1)} = 1 \pm \sqrt{I-L} \tag{17}$$

where

$$L = 2\bar{u}_L - 1 \tag{18}$$

Several points are to be observed at once with regard to equation (17). First of all, the discriminant must always be positive in order to obtain real values for $\bar{u}$, thus

$$I \geq L \tag{19}$$

Furthermore, the choice of plus or minus sign determines whether the local velocities are subsonic or supersonic. A change in sign at the point where the radical is zero corresponds to a smooth transition through sonic velocity. A change in sign at a point where the radical is not zero results in a discontinuous jump in velocity and corresponds physically to a shock wave. Such discontinuities are permissible when they proceed from supersonic to subsonic velocities (or from plus to minus sign in eq. (17)) when progressing in the flow direction. Discontinuities in the reverse direction are inadmissible since they correspond to expansion shocks, a phenomenon which violates the second law of thermodynamics.

In order to remove unnecessary complications and to facilitate the discussion, the following remarks are confined to the relations among I, L, $\bar{u}$, and $\bar{u}_L$ evaluated at the airfoil surface. In this way, each of the four functions reduces to a function of a single variable $\bar{x}$ and can be illustrated simply by curves rather than by surfaces. The subscript W is appended to each of the four variables to denote that the values are those at the wing surface. The L_W and I_W curves represent the components involved in the solution of equation (17), and $\bar{u}_W$ and $\bar{u}_{L_W}$ curves represent, respectively, the velocity distributions given by transonic theory and by linear theory.

The linear theory solution $\bar{u}_{L_W}$ for subsonic flow around a nonlifting airfoil of given shape can be readily derived through application of equation (14). The corresponding values for the L_W curve follow directly from equation (18). Not very much can be stated at this point about the values for I_W, except that they depend on the distribution as well as magnitude of $\bar{u}$ and that the inequality mentioned above must be satisfied. The relation between the I_W and L_W curves is of utmost importance, however, and will be discussed qualitatively in the following paragraphs.

It follows from the discussion presented in the preceding paragraphs that the qualitative features of the relations among the I_W, L_W, $\bar{u}_W$, and $\bar{u}_{L_W}$ curves are of essentially one form for flows in which the free-stream Mach number is less than the critical, and of another form for flows in which it is greater than the critical. If the Mach number is less than the critical, the I_W and L_W curves never touch. Sketches of typical curves for this condition are shown in sketch (b). The amplitudes of all four curves increase as the free-stream Mach number increases, however, and the I_W and L_W curves finally touch at one point as the free-stream Mach number becomes equal to the critical Mach number. If the free-stream Mach number is greater than the critical, the I_W and L_W curves must continue to touch at least one point along the chord in order to avoid the occurrence of forbidden expansion shock waves. The two curves may also be tangent at a second

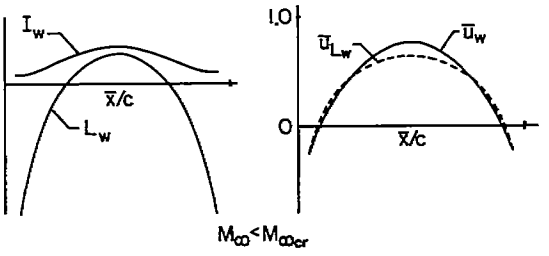

Sketch (b)

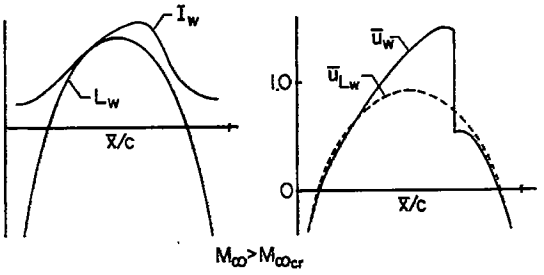

Sketch (c)

point along the chord, in which case the flow may decelerate smoothly from supersonic to subsonic velocities. All present indications are that such flows are very exceptional if they exist at all, and that, in most cases, the flow decelerates abruptly from supersonic to subsonic velocities through a shock wave. For these cases, the I_W and L_W curves are tangent at only one point along the chord and the four curves appear qualitatively as illustrated in sketch (c). The point of tangency locates the position of the sonic point and the point at which the sign in equation (17) changes from minus to plus. At some point downstream of the sonic point, the flow decelerates abruptly to subsonic velocities and the sign in equation (17) changes back to minus. If the I_W and L_W curves are continuous at this point, the jump in $\bar{u}_W$ is from $1 + \Delta$ to $1 - \Delta$, corresponding to that of a normal shock wave, and $(d\bar{u}_W/d\bar{x})_a = -(d\bar{u}_W/d\bar{x})_b$.

Simplification of the Integral Equation

Since no general methods are available for the solution of integral equations, such as equation (13), that are both nonlinear and singular, recourse must be had to approximate methods. Approximate solutions of this equation could conceivably be worked out numerically by starting with a two-dimensional grid of suitably selected values for $\bar{u}(\bar{\xi},\bar{\zeta})$ and iterating until convergence is obtained. Such calculations would proceed by inserting the assumed values for $\bar{u}$ into the double integral and solving to obtain the next approximation for $\bar{u}(\bar{x},\bar{z})$, making use of tangency condition on the surfaces or functions represented by I and L as discussed in the preceding paragraphs. If the first approximation for $\bar{u}$ is taken to be $\bar{u}_L$, it is shown in the appendix of reference 1 that the final result for $\bar{u}$, in the limit of an infinite number of iteration steps, coincides with that provided by classical iteration methods, provided the free-stream Mach number is less than the critical. It is shown, furthermore, that the power series expansions for the higher approximations to the solutions of the equations of transonic flow theory obtained by application of classical iteration methods diverge if the free-stream Mach number is greater than the critical.

The method of reference 1 does not seek approximate solutions for supercritical flows by taking $\bar{u}_L$ to be the first approximation, but follows an idea of Oswatitsch expressed in references 6 and 7 that approximate solutions for mixed flows containing shock waves can be obtained if the starting $\bar{u}$ distribution contains discontinuities compatible with the shock relations. This idea is combined in reference 1 with an iteration procedure that incorporates the considerations described above regarding the relation between the I and L functions. It is shown further in

reference 1 that this procedure converges rapidly and that it is not necessary to be highly accurate in the selection of initial values for u, provided care is exercised in fulfilling the tangency requirement on the I and L functions.

A source of complication in the numerical solution of equation (13) by an iteration process is the double integral. It is assumed in the method of reference 1 that approximate knowledge of the velocity distribution in space is sufficient for determining a working approximation for the double integral. The possibility of introducing simplifying approximations in an integral, with the effect that the error in the result may be rather small, appears to be the principal advantage of approaching the nonlinear problems of compressible flow theory, and perhaps other problems as well, through consideration of an integral equation rather than through direct consideration of a differential equation.

The particular assumption introduced at this point in the method of reference 1 is that a sufficiently good approximation to the velocities in the flow field surrounding the airfoil can be expressed in terms of the local coordinate $\bar{z}$, the ordinates of the airfoil surface $\bar{Z}(\bar{x})$, and the desired, but unknown velocity distribution $\bar{u}_w(\bar{x})$ on the airfoil surface. This permits one integration to be performed, thereby reducing the double integral of equation (13) to a single integral. The particular expression used in reference 1 and in the calculations of additional results reported in this paper is one suggested originally by Oswatitsch in references 6 and 7. It possesses the properties that $\bar{u}$ starts from the value $\bar{u}_w$ at the airfoil surface ($\bar{z} = 0$) with an initial rate of change given by the irrotationality condition and vanishes at great distances as $1/\bar{z}^2$, and is explicitly the following:

$$\bar{u}(\bar{x},\bar{z}) = \frac{\bar{u}_w(\bar{x},0)}{[1+(\bar{z}/b)]^2} \tag{20}$$

where

$$b = -\frac{2\bar{u}_w}{\partial^2\bar{Z}/\partial\bar{x}^2}$$

Substitution of equation (20) in the double integral of equation (13) permits integration with respect to $\bar{\zeta}$. Thus, by performing this integration and setting $\bar{z} = 0$, the following approximate integral equation is obtained for $\bar{u}_w$:

$$\bar{u}_w = \bar{u}_{I_w} + \frac{\bar{u}_w^2}{2} - \int_0^c \frac{\bar{u}_w^2}{2b} E\left(\frac{\xi-\bar{x}}{b}\right) d\xi \tag{21}$$

The function E is

$$E\left(\frac{\bar{\xi}-\bar{x}}{b}\right) = E(X) = \frac{4}{\pi(1+X^2)^5}\left[\frac{\pi}{2}|X|(5-10X^2+X^4) - (1-10X^2+5X^4)\ln|X| - \frac{1}{12}(1+X^2)(25-71X^2-X^4-X^8)\right] \quad (22)$$

Although the integration interval is indicated in equation (13) to extend from $\bar{\xi} = -\infty$ to $\bar{\xi} = +\infty$, the contribution of the regions ahead of the leading edge and behind the trailing edge vanishes with the introduction of the velocity profile given by equation (20) since b is infinite. The integration need, therefore, be carried out only over the chord c.

Attention is called to the fact that the approximate relation for $\bar{u}(\bar{x},\bar{z})$ given by equation (20) is not entirely satisfactory. Evidence of this is provided by the facts that $\bar{u}$ is indicated to be zero in the region ahead of the leading edge and behind the trailing edge where b is infinite and that the discontinuities in $\bar{u}$ at the shock waves are consistent with the shock relations only at the surface of the airfoil. A further shortcoming of equation (20) is that it cannot be used in a region where b is negative since it leads to a spurious infinity when inserted into the integral of equation (13). For the convex airfoils considered in this paper, negative values for b are indicated by the above expression for small regions near the leading and trailing edges where $\bar{u}_w$ is negative. Since estimates indicate that the contributions of these regions to the value of the double integral are very small over most of the chord compared with those of the regions in the middle of the airfoil, the contributions of regions where $\bar{u}$ is negative have been consistently disregarded in the present calculations.[1]

Negative values for b also result in regions of positive $\bar{u}_w$ if the adjacent surface of the airfoil is concave rather than convex. This situation does not arise in the cases considered in this paper because all of the airfoils have convex surfaces, but is likely to occur in other cases, a typical example being that of supercritical flow past an airfoil with a cusped trailing edge. In this particular case, the positive values of $\bar{u}_w$ and the chordwise extent of the region of negative b may be large, and the simple expedient of disregarding the influence of such regions could hardly be expected to succeed. It would appear necessary, before pressure distributions are calculated for such cases, to reconsider the question of a suitable velocity profile and to introduce some other

[1]This point was improperly observed in the calculation of the results for the symmetrical circular-arc airfoils given originally in reference 1. The results for this airfoil that are presented herein have been corrected to conform with the above statement, even though the difference between the two sets of results is generally quite small.

expression more appropriate than that given by equation (20). The same conclusion applies also to airfoils with extensive flat regions for which b is infinite.

The error δI incurred in the value of I by the introduction of the relation between $\bar{u}$ and $\bar{z}$ given by equation (20) is, of course, equal to the difference between the exact and approximate values for I, that is,

$$\delta I = I_{ex} - I_{app} = \int_{-\infty}^{+\infty}\int q_{ex}\sigma \, d\bar{\xi} \, d\bar{\zeta} - \int_{-\infty}^{+\infty}\int q_{app}\sigma \, d\bar{\xi} \, d\bar{\zeta} = \int_{-\infty}^{+\infty}\int (q_{ex} - q_{app})\sigma \, d\bar{\xi} \, d\bar{\zeta} \qquad (23)$$

where

$$\sigma = \frac{\partial^2}{\partial \bar{\xi}^2} \ln \frac{1}{r_2} \qquad q_{ex} = \frac{\bar{u}^2}{2\pi} \qquad q_{app} = \begin{cases} \dfrac{\bar{u}_w^2}{2\pi[1+(\bar{\zeta}/b)]^4} & \text{for } b > 0 \\ 0 & \text{for } b < 0 \end{cases}$$

These expressions possess two properties that make it difficult to estimate upper bounds for the magnitudes of I_{ex} and I_{app}. They are that the region of integration extends to infinity and that σ is singular, or infinite, at $\bar{\xi} = \bar{x}$, $\bar{\zeta} = \bar{z}$. In actual applications, however, the first property does not lead to large contributions from the distant regions because q_{ex} diminishes sufficiently rapidly with distance from the airfoil, and q_{app} is chosen so as to assure the same behavior. The second property remains a factor, however, because neither q_{ex} nor q_{app} vanishes at the singular point of σ. Although it is one of the principal properties of the integral equation given by equation (13) that serious difficulties arising from this source are averted by the fact that the values of σ change from positive to negative in a cyclic manner as the point $\bar{\xi},\bar{\zeta}$ moves around the singular point $\bar{x},\bar{z}$, it is nevertheless true that most of the contribution to the value of I arises from the region in the vicinity of $\bar{x},\bar{z}$. It appears plausible, however, since q_{app} has the same values and first derivatives as q_{ex} for all points along the airfoil chord, except those in the immediate vicinity of the leading and trailing edges, that the error incurred in the value of I should be small for some large class of smooth convex airfoils.

It is shown in reference 1 and verified further by examination of the new results presented herein that considerations based on the use of equation (21) together with the relation between the I and L curves discussed in the preceding section lead to useful results for all Mach numbers up to that at which the shock wave is situated at the trailing

edge of the airfoil. At higher Mach numbers, the approximation furnished by equation (21) is inadequate, particularly for the region near the trailing edge, because of the presence of a pair of oblique shock waves extending downstream from the trailing edge. Examination of the properties of I_{ex} in the presence of such a shock system shows that there is a logarithmic singularity at the trailing edge that exactly counteracts the singularity in $\bar{u}_L$, and a discontinuity in its value elsewhere along the shock wave. This point was not understood at the time reference 1 was prepared and an attempt was made there to obtain results for higher Mach numbers by assuming that an adequate approximation for the contribution of the double integral to the values of $\bar{u}$ on the airfoil could be attained by replacing the actual oblique shock system with a normal shock wave situated at the trailing edge. This procedure yielded results for the pressure distribution on the airfoil that appeared reasonable in spite of the occurrence of a logarithmic singularity in $\bar{u}$ at the trailing edge. This singularity arose from the fact that the approximation introduced by use of I_{app} resulted in the loss of the singularity in I, and therefore provided no mechanism for the proper cancellation of the singularity in $\bar{u}_L$. An additional difficulty that arose in reference 1 in this Mach number range is associated with the fact that no direct plan for iteration could be devised and that approximate solutions had to be sought by using a procedure that might be described as partly iteration and partly trial and error. Although it would be desirable to develop the present approach so that results could be obtained for the entire Mach number range, this has not yet been done because results for Mach numbers near unity can now be obtained by application of the newer and simpler approximate methods of reference 2. The present results, together with those given in reference 2, cover the entire Mach number range from zero to somewhat greater than unity with only a small gap remaining for Mach numbers equal to or slightly larger than that at which the shock wave reaches the trailing edge.

Numerical Evaluation of Integral

One of the principal steps in the iteration method described in reference 1 is the evaluation of the integral involved in equation (21). Since $\bar{u}_W$ and b are generally prescribed by a set of numerical values rather than by analytic functions, a numerical technique has been used for the integration. The process consists of replacing the prescribed $\bar{u}_W$ distribution by a stepwise approximation as indicated in sketch (d), introducing a mean value for b for each of the rectangular elements, integrating to determine the contribution of a single element, and summing the influence of all elements for which b is positive. The contribution of a single element of width l and centered at $\bar{x} = \bar{\xi}_1$, as typified by the shaded area of sketch (d), is given by

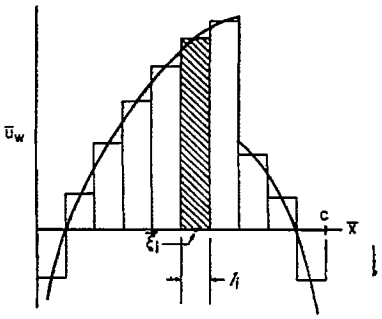

Sketch (d)

$$\frac{\bar{u}_{W_i}^2}{2} f\left[\left(\frac{\bar{x}-\bar{\xi}_i}{l_i}\right), \left(\frac{2l_i}{b_i}\right)\right] = \frac{\bar{u}_{W_i}^2}{2b_i} \int_{\bar{\xi}_i - \frac{l_i}{2}}^{\bar{\xi}_i + \frac{l_i}{2}} E\left(\frac{\bar{\xi}-\bar{x}}{b_i}\right) d\bar{\xi} \tag{24}$$

Upon performance of the indicated operations, the following expression is obtained for f:

$$\frac{\pi}{4} f = \frac{1}{12(1+A^2)^4}\left\{\frac{3\pi}{2}\frac{A}{|A|}\left[(1+A^2)^4-(1+A^2)^2+8(1+A^2)-8\right]+\right.$$

$$\left.12A(A^2-1)\ln|A|-A(1+A^2)\left[(1+A^2)^2+12\right]\right\}+$$

$$\frac{1}{12(1+B^2)^4}\left\{\frac{3\pi}{2}\frac{B}{|B|}\left[(1+B^2)^4-(1+B^2)^2+8(1+B^2)-8\right]+\right.$$

$$\left.12B(B^2-1)\ln|B|-B(1+B^2)\left[(1+B^2)^2+12\right]\right\} \tag{25}$$

where

$$A = \frac{l_i+2(\bar{x}-\bar{\xi}_i)}{2b_i}, \qquad B = \frac{l_i-2(\bar{x}-\bar{\xi}_i)}{2b_i}$$

Thus, the integral in equation (21) is approximated as follows:

$$\int \frac{\bar{u}_W^2}{2b} E\left(\frac{\bar{\xi}-\bar{x}}{b}\right) d\xi = \sum \frac{\bar{u}_{W_i}^2}{2} f\left[\left(\frac{\bar{x}-\bar{\xi}_i}{l_i}\right), \left(\frac{2l_i}{b_i}\right)\right] \tag{26}$$

A graph illustrating the variation of f with $2l_i/b_i$ for various $(\bar{x}-\bar{\xi}_i)/l_i$ is given in reference 1 and is not repeated here.

Most of the results given in reference 1 were calculated using only 10 elements to approximate the $\bar{u}_W$ curve. That this number is sufficient for the symmetrical circular-arc airfoil was checked by repeating the calculations in selected cases using 20 elements and noting

that the results were nearly indistinguishable on the scale to which they are presented in reference 1. The same general procedures were followed at the outset of the calculations of the pressure distributions for the additional airfoils included in the present investigation. It was gradually concluded, however, that the extra work incurred by the use of 20 rather than 10 elements is largely compensated by the more rapid convergence of the iteration process, and that in many cases less total work is required to perform the calculations with the larger number of elements. As a result, all of the pressure distributions presented for the airfoils having maximum thickness at 30- and 70-percent chord were calculated using 20 elements. On the other hand, the pressure distributions for the airfoils having maximum thickness at 40- and 60-percent chord were calculated using 10 elements for all Mach numbers except the critical, for which 20 elements were used.

Determination of $\bar{u}_{L_W}$

The values for $\bar{u}_{L_W}$ can be determined from the general solution for $\bar{u}_L$ given in equation (14) by performing the indicated operations and setting $\bar{z} = 0$, or more simply from the following expression derived from equation (14):

$$\bar{u}_{L_W} = \frac{1}{\pi} \int_0^c \frac{d\bar{Z}}{d\bar{\xi}} \frac{d\bar{\xi}}{\bar{x}-\bar{\xi}} \tag{27}$$

The Cauchy principal value is used in the integration. In this way, the following expression is obtained for $\bar{u}_{L_W}$ for the airfoils described by equations (1) and (2):

$$\bar{u}_{L_W} = \frac{\bar{\tau}}{2\pi} \frac{n^{n/(n-1)}}{n-1} \left\{ \left[1-n\left(\frac{\bar{x}}{c}\right)^{n-1} \right] \ln \frac{\bar{x}}{c-\bar{x}} + n \left[\frac{1}{n-1} + \frac{1}{n-2}\left(\frac{\bar{x}}{c}\right) + \cdots + \frac{1}{n-m+1}\left(\frac{\bar{x}}{c}\right)^{m-2} + \left(\frac{\bar{x}}{c}\right)^{m-1} \int_0^1 \frac{\left(\frac{\bar{x}}{c}\right)^{n-m} - \left(\frac{\bar{\xi}}{c}\right)^{n-m}}{\frac{\bar{x}}{c} - \frac{\bar{\xi}}{c}} d\left(\frac{\bar{\xi}}{c}\right) \right] \right\} \tag{28}$$

where m is such an integer that $0 \leq (n-m) < 1$. If n is any integer, $n-m$ is zero and the integral disappears. Thus equation (28) reduces to the following simple form for the symmetrical circular-arc airfoil for which $n = 2$:

$$\bar{u}_{L_W} = \frac{2\bar{\tau}}{\pi}\left[\left(1-2\frac{\bar{x}}{c}\right)\ln\frac{\bar{x}}{c-\bar{x}} + 2\right] \tag{29}$$

If n is not an integer, the integral remains. It can be evaluated analytically if n is any integer plus certain simple fractions. In the present investigation, however, it is necessary to consider the values 3.38 and 6.05 for n and the integrals are evaluated numerically. No difficulty occurs at the point where $\bar{\xi} = \bar{x}$ since the integrand is not singular but is equal to $(n-m)/(\bar{x}/c)^{1-(n-m)}$. The general expression for $\bar{u}_{L_W}$ for the airfoils described by equations (2) and (3) can also be written in a similar manner, but it is sufficient to note that the results are the same, except for replacement of $\bar{x}/c$ by $1-(\bar{x}/c)$, as those found by application of equation (28). The chordwise variation of $\bar{u}_{L_W}$ for each of the five airfoils of the present investigation is shown graphically in sketch (e).

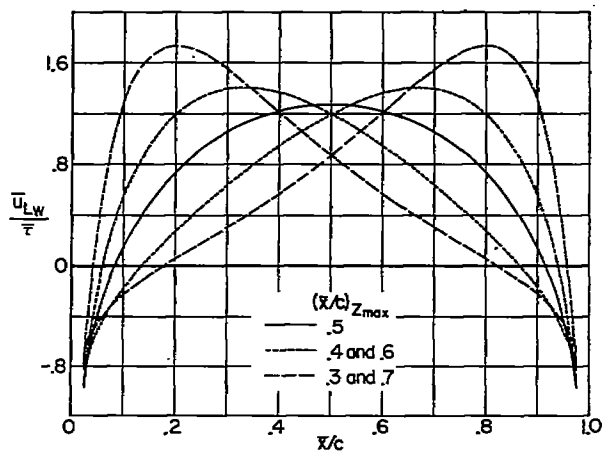

Sketch (e)

Iteration Solution of Integral Equation

Approximate results for pressure distributions on thin airfoils are determined, in the method of reference 1, by solving the simplified integral equation by use of an iteration procedure in which certain operations at each step are performed numerically and other operations are performed graphically. In particular, the value of the integral, or the function designated in the above discussion by I, is determined numerically; the tangency condition between the I and L functions is satisfied, when necessary, by use of graphical technique; and the resultant values for $\bar{u}_W$ are determined at each step by use of the quadratic formula as indicated by equation (17). These techniques have been applied without modification in the calculation of the new results presented in this paper. It should be remarked, however, that there are two categories of problems discussed in reference 1 for which no new results are given in this paper. One of these is that of shock-free supercritical flows for which no further attempts were made to attain solutions because it seemed evident that the same negative result reported in reference 1 would again be found. The other category is the one mentioned previously that includes the Mach number range near unity at which the shock wave is situated at the trailing edge and the approximation of the variation of $\bar{u}$ with $\bar{z}$ furnished

by equation (20) is clearly inadequate. In spite of this known deficiency and the lack of a direct plan of iteration, numerous calculations were actually made for this category. Although the quality of the results was generally comparable with that of the corresponding results reported in reference 1 for the symmetrical circular-arc airfoil, it was not equal to the quality of the results for lower Mach numbers. This situation, together with the decreased necessity for the results occasioned by the development of the theory of reference 2, has caused these results to be omitted from the present report.

The two categories for which new results are given in this paper are (a) subcritical flows and (b) supercritical flows for which the shock wave is situated forward of the trailing edge. The details of the iteration method are such that the Mach number or value of ξ_∞ for a given calculation can be selected in advance for subcritical flows, but not for supercritical flows. In the latter case, the position of the shock wave is fixed instead, and the associated Mach number is found as part of the solution. For this reason, results given for supercritical flows are selected so that the shock wave is situated at even intervals of the chord, rather than so that there are even intervals of Mach number or ξ_∞.

RESULTS AND DISCUSSION

Presentation of Results

The theory described in the preceding pages has been applied to calculate pressure distributions for both subcritical and supercritical Mach numbers on each of the five families of airfoils described at the beginning of this paper. As noted previously herein, the Mach number range investigated extends in each case from well below the critical up to the lowest Mach number at which the shock wave is at the trailing edge. The results are given in numerical form in table I and are illustrated graphically in figures 1 through 5. Each figure consists of two parts. Part (a) presents the results for subcritical flows and part (b) presents the results for supercritical flows.

As indicated previously herein, the pressure distribution associated with the value of ξ_∞ for which the shock wave is situated at the trailing edge is inaccurate in the vicinity of the trailing edge. The results presented for this case are consequently indicated by a dashed line over the last few percent chord.

In addition to the above results, each part of each figure contains an extra set of results indicated by a dotted line that is useful for reference and comparison. The dotted line in part (a) of each figure indicates the pressure distribution provided by linear theory for the lowest Mach number (or most negative ξ_∞) considered for each airfoil. That in part (b) of each figure indicates the theoretical pressure

distribution given in reference 2 for free-stream Mach number 1 ($\xi_\infty = 0$). The latter results are shown in reference 2 to be in substantial agreement with the experimental results of references 3 and 4.

Examination of the results for the various airfoils reveals that the pressure distributions for supercritical flows bear an interesting relation to the pressure distributions for the critical Mach number and for free-stream Mach number 1. As the Mach number is increased beyond the critical, the shock wave increases in strength and moves rearward across the chord, but the values of $\overline{C}_p$ over the forward portions of the airfoil remain nearly the same as at the critical Mach number. When the Mach number is increased sufficiently that the shock wave reaches the trailing edge, the entire pressure distribution resembles in form, but not in level, the pressure distribution at Mach number 1. It can be seen, however, that the chordwise extent of the supersonic region and the rate at which it grows as the Mach number is increased beyond the critical are strongly dependent on the shape of the airfoil. These statements are illustrated by the curves provided in sketch (f) that show the variation with ξ_∞ of the locations of the sonic point and the shock wave for each of the airfoils. The dotted lines for values of ξ_∞ near zero refer again to the results given in reference 2 for the location of the sonic point at Mach number 1 and vicinity.

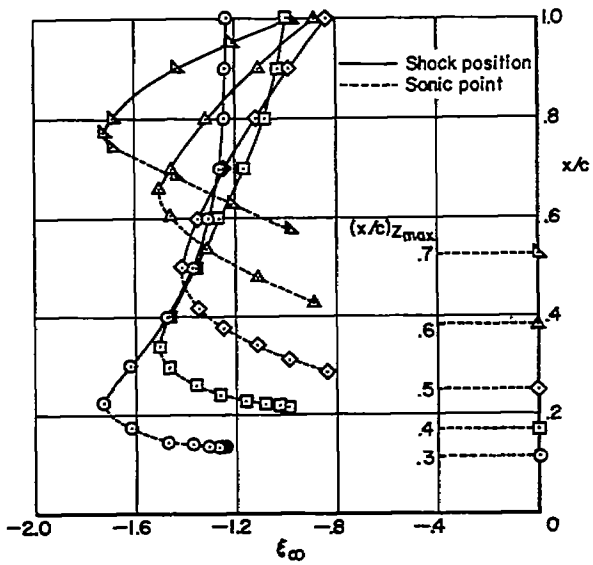

Sketch (f)

The results for the airfoil having maximum thickness at 30-percent chord are particularly interesting because they indicate that the position of the shock wave changes very rapidly with small changes in ξ_∞ or Mach number. It is possible that this result may have a bearing on some of the unsteady conditions that are observed in experimental investigations (see, for instance, ref. 8). These conditions are generally associated with extensive shock-wave boundary-layer interaction. The circumstances encountered on the airfoil with the point of maximum thickness at 30-percent chord suggest that unsteady phenomena of major importance may also occur even in inviscid flows if there is a little unsteadiness in the main stream. The circumstances associated with this airfoil are in marked contrast to those for the other airfoils considered herein for which the position of the shock wave is more strongly dependent on ξ_∞.

Examination of the simplified integral equation given in equation (21) discloses that the great sensitivity of the shock position to small changes in Mach number exhibited by the results for the airfoil with maximum

thickness at 30-percent chord is not to be associated, in general, with a forward location of the point of maximum thickness, but with a vanishing of the curvature of the rear portion of the airfoil. This conclusion follows directly from the fact that the contribution to the value of the integral of equation (21) arising from such regions is very small because b is large according to equation (20), $E[(\bar{\xi}-\bar{x})/b]$ is large logarithmically according to equation (22), and the quotient E/b in the integrand vanishes in the limit as the curvature approaches zero. It thus follows that the I curve, hence the $\bar{u}_{I_W}$ curve, and finally the free-stream Mach number are very insensitive to variations in the location of the shock wave if the shock wave is situated adjacent to a part of the airfoil where the curvature is very small. Although this conclusion appears to be a general property of the simplified integral equation given in equation (21), some caution should be exercised in its immediate acceptance and widespread application to physical problems because the approximate relation, equation (20), introduced in the development of equation (21) from the exact integral equation given in equation (13) obviously deteriorates in quality as the curvature vanishes. The agreement between the present results and those for Mach numbers near 1 given in reference 2 suggests, however, that the quality of the specific results given in this paper is not unduly impaired by this factor.

The results given in figures 1 through 5 are presented again in figures 6 through 10 in an alternative form in which the variation of $\bar{C}_p$ with ξ_∞ is plotted for various stations along the chord. This form of presentation is the counterpart, in terms of reduced quantities, of the plots commonly given in reports of experimental investigations showing the variation of C_p with M_∞ at prescribed points on the surface of a wing or body. An additional set of lines is included on each of these figures showing the theoretical results given in reference 2 for the variation of $\bar{C}_p$ with ξ_∞ for free-stream Mach numbers near 1. It can be seen that these results are in essential agreement with those calculated by the method of reference 1 for lower Mach numbers. This agreement is of particular interest because the two sets of results have been calculated by methods that are new and approximate, but that differ widely in the details of the approximation.

It is evident from examination of figures 1 through 10 that the results calculated by the method of reference 1 display the anticipated qualitative aspects of transonic flows associated with the part of the Mach number range to which they apply (i.e., appearance, rearward movement, and increase in strength of the shock wave as the Mach number is increased beyond the critical, etc.) and are in good quantitative agreement with other theoretical results for low Mach numbers and for Mach numbers near unity. The remaining sections of this paper are concerned with comparisons of the present results with those of higher order theory for subcritical flows and with those of experiment for supercritical flows.

The results given in figures 1 through 10 are all expressed in terms of $\bar{C}_p$ and ξ_∞. Since the extraction of the value of M_∞ that is associated with a given pair of values for ξ_∞ and the thickness ratio τ

requires the solution of a cubic algebraic equation and is somewhat inconvenient, figure 11 has been included to give the variation of M_∞ with ξ_∞ for various τ. It is assumed in the preparation of this graph that γ is 7/5.

Comparison With Existing Higher Approximations for Subcritical Flows

Although the results for supercritical flows represent the primary contribution of the present investigation, it is not without interest to examine the results for subcritical flows in somewhat greater detail and to compare them with existing results given by linear theory and by higher approximations. These comparisons are of particular importance in the present discussion because it is only for subcritical flows that a good evaluation of the degree of accuracy of the results can be achieved at the present time. Even this discussion is handicapped somewhat by the fact that all other theories for subsonic flow around airfoils are also approximate and that no exact solutions are known.

From the present point of view, the most significant method that has been used to obtain higher approximations to the solution for subcritical flow around thin airfoils is the method of successive approximation in which the solution is expressed in a power series in thickness ratio. In this method, the first term is the result given by linear theory, and the coefficients of successive terms are determined by iteration. Although a general procedure for the evaluation of the second approximation has recently been given by Van Dyke (ref. 9), the determination of the third approximation has been accomplished for only a few special shapes. One of these is the nonlifting symmetrical circular-arc airfoil for which the second approximation has been given by Hantzsche and Wendt (ref. 10) and the third approximation by Asaka (refs. 11, 12, and 13).[2] Sketch (g) shows a comparison of the variations of C_p with M_∞ at the midpoint of such an airfoil having a thickness ratio τ of 0.10, as indicated by the present calculations and by the first, second, and third approximations. It can be seen that the present results approach those given by the first

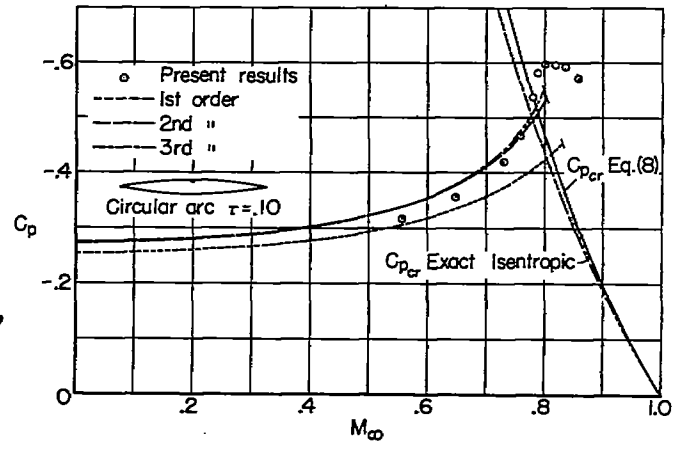

Sketch (g)

[2]The results for the third approximation given in the present report differ from those obtainable directly from the expressions given in either references 11 or 12 and 13 because of the correction of some misprints. These corrections have been verified by correspondence with the author.

approximation (or linear theory) for small Mach numbers, but depart therefrom with increasing Mach number and are much closer to the higher approximations for Mach numbers near the critical. At Mach numbers greater than the critical, the results of the present calculations differ markedly from those indicated by the method of successive approximation. This is proper, however, since the range of applicability of the latter method is confined to subcritical Mach numbers.

It should be noted that the curves labeled first, second, and third order present the results indicated by successive approximations to the solution of the exact equations for inviscid compressible flow. It is of greater significance, from the point of view of evaluating the accuracy of the present calculations, to compare the present results with those indicated by successive approximations to the solution of the simplified equations of transonic small-disturbance theory. The latter results can be calculated by use of the following expression, which is readily derived from Asaka's result by taking the limiting form consistent with the approximations of transonic flow theory:

$$\frac{(U_\infty k)^{1/3}}{\tau^{2/3}} C_{p_n} = \overline{C}_{p_n} = -\sum_{m=0}^{n} a_m \left(-\frac{1}{\xi_\infty}\right)^{(3m-2)/2} \tag{30}$$

where for the midpoint of a circular-arc airfoil

$$\left.\begin{aligned} a_0 &= 0 \\ a_1 &= \frac{8}{\pi} = 2.5465 \\ a_2 &= \frac{10}{\pi^2} - \frac{1}{2} = 0.5132 \\ a_3 &= \frac{1}{\pi}\left(-\frac{281}{108} + \frac{7}{6}\ln 2\right) + \frac{1}{\pi^3}\left(\frac{292}{9} + 4.908\right) = 0.6339 \end{aligned}\right\} \tag{31}$$

Notice that $\overline{C}_{p_0} = 0$ and $\overline{C}_{p_1} = \overline{C}_{p_L}$. It can be seen from the graphical display of the results given in sketch (h) that the variation of C_p with M_∞ indicated by the present calculations is slightly greater than that indicated by the third approximation. The precise evaluation of the accuracy of the present results remains uncertain because neither the exact solution nor an upper bound for the results is provided by the classical method of successive approximations.

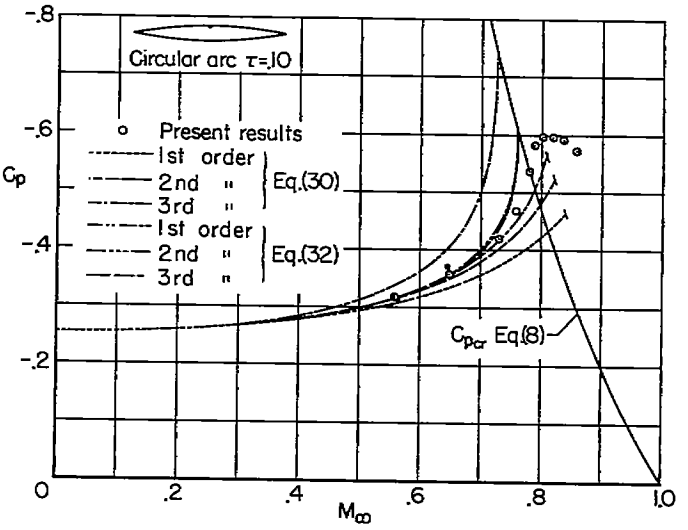

Sketch (h)

In order to provide further insight into this situation, three additional curves are included in sketch (h) to show the variations of C_p with M_∞ indicated by the following expression:

$$\frac{(U_\infty k)^{1/3}}{\tau^{2/3}} C_{p_N} = \overline{C}_{p_N} = 2\xi_\infty \left[1 - \sqrt{\left(1 - \frac{\overline{C}_{p_{n-1}}}{2\xi_\infty} \right)^2 - \frac{\overline{C}_{p_n} - \overline{C}_{p_{n-1}}}{\xi_\infty}} \right]$$

$$= 2\xi_\infty \left[1 - \sqrt{\left(1 - \frac{\overline{C}_{p_{n-1}}}{2\xi_\infty} \right)^2 - a_n \left(-\frac{1}{\xi_\infty} \right)^{3n/2}} \right] \qquad (32)$$

where for the midpoint of a circular-arc airfoil the coefficient, a_n, is given in equation (31). Notice that

$$\left.\begin{aligned} \overline{C}_{p_{N=0}} &= 0 \\ \overline{C}_{p_{N=1}} &= 2\xi_\infty \left[1 - \left(1 - \frac{\overline{C}_{p_L}}{\xi_\infty} \right)^{1/2} \right] \end{aligned}\right\} \qquad (33)$$

The foregoing expressions represent the results of the Nth approximation obtained by application of an alternative method of successive approximations that involves the solution of quadratic rather than linear equations at each step of the iteration process. This method, described

briefly in reference 1 and discussed at greater length in reference 2, yields results at each step that overestimate, rather than underestimate, the variation with M_∞ of the peak negative values for C_p. Although the difficulties of integration are as great as in the classical method of successive approximations and only the first few steps can be evaluated in any specific application, it is shown in the appendix of the report version of reference 1 that the results obtained for flows that are subsonic everywhere converge, in the limit of an infinite number of iteration steps, to the same result as ultimately obtained by application of the classical method of successive approximations. The result obtained by application of the quadratic method clearly terminates with the occurrence of sonic velocity somewhere in the flow field, however, and no results are provided for mixed or transonic flows. This termination of the result is in distinct contrast to the apparent behavior of the results of the classical method of successive approximation, but closer examination of the relation between the two sets of results reveals that the infinite series with which the latter results are expressed does not converge at Mach numbers greater than the critical and that the values indicated for transonic flows are false. Since the exact solution of the equations of transonic flow theory is presumed to indicate a variation of C_p with M_∞ that is somewhat greater than that indicated by the third approximation of the classical method, but somewhat less than that indicated by the third approximation of the quadratic method, it is evident upon examination of sketch (h) that the proper trend is defined within rather narrow limits, and that the results of the present numerical calculations fall within these limits.

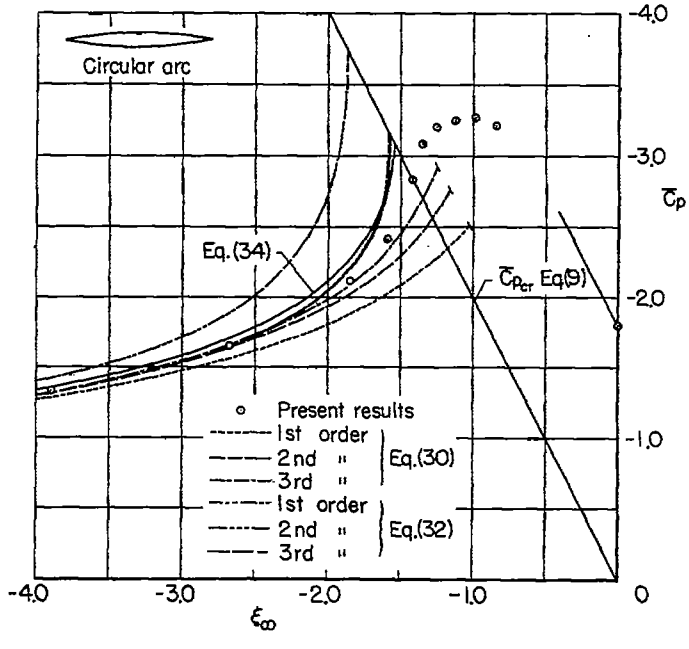

Sketch (i)

Although it is immediately evident from the foregoing discussion that results corresponding to those illustrated in sketch (h) for the 10-percent-thick airfoil could be calculated readily for airfoils of other thickness ratios, graphical presentation of the results in terms of C_p and M_∞ would require a complete set of curves for each thickness ratio considered. The corresponding values for thin airfoils of arbitrary thickness ratio can be summarized concisely by a single set of lines, however, by plotting the results in terms of the reduced variables $\bar{C}_p$ and ξ_∞. Such a plot is given in sketch (i). It can be seen that the relationship between the various approximations remains substantially the same as illustrated in sketch (h) for the special case of a 10-percent-thick airfoil.

The corresponding results for the variation of $\bar{C}_p$ with ξ_∞ at the station, x/c, along the chord at which the present results indicate sonic velocity is first attained as the Mach number is increased are shown for the other four airfoils of the present investigation in sketches (j) and (k). It is necessary to present only two plots because the results for subcritical Mach numbers are the same for the airfoils having the point of maximum thickness located at 30- and 70-percent chord, and similarly for those having maximum thickness at 40- and 60-percent chord. Since approximations higher than the first have not been determined for comparison with the present numerical results for the latter four airfoils, an additional curve is included in sketches (i), (j), and (k) illustrating the variation of $\bar{C}_p$ with ξ_∞ indicated by the following pressure-correction formula derived in reference 2:

$$\bar{C}_p = 2\xi_\infty \left[1 - \left(1 - \frac{3}{4} \frac{\bar{C}_{p_L}}{\xi_\infty} \right)^{2/3} \right] \tag{34}$$

where $\bar{C}_{p_L}$ is the value for $\bar{C}_p$ indicated by linearized compressible flow theory. The relation given by equation (34) is approximate, but it can be seen from sketch (i) that its use leads to results that are more accurate than those indicated by linearized theory. Although it has not been proved in general, it appears from examination of the results for the symmetrical circular-arc airfoil and other cases for which higher order approximations are available that the variation of $\bar{C}_p$ with ξ_∞ indicated by equation (34) is somewhat greater than the proper trend.

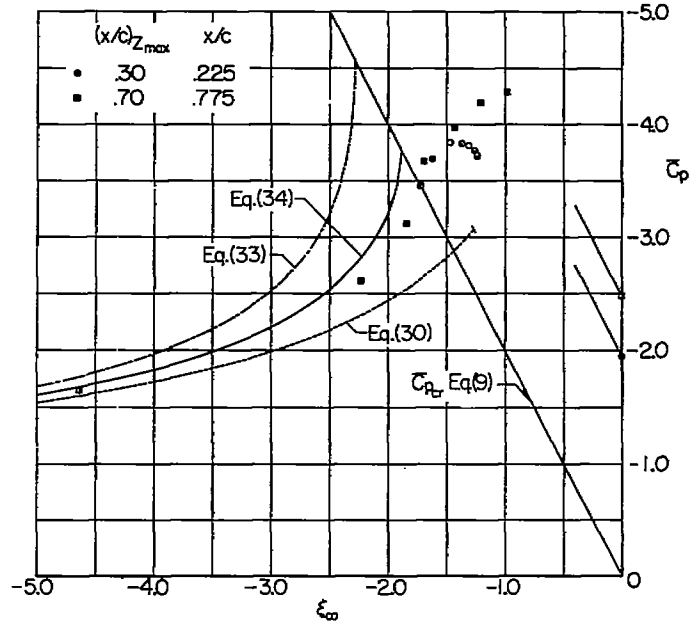

Sketch (j)

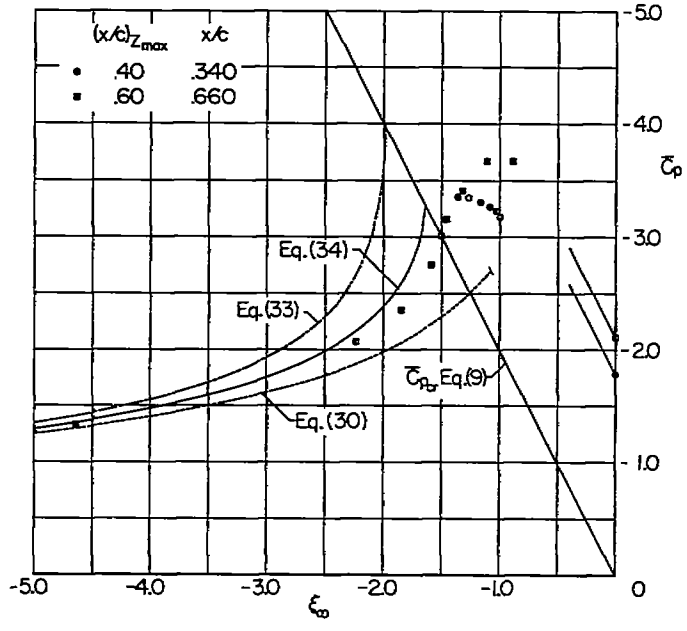

Sketch (k)

It can be seen from the foregoing comparisons that the present numerical results appear in each case to be in good accordance with other theoretical results for subcritical Mach numbers. There are no corresponding theoretical results available with which the present results for supercritical Mach numbers can be compared, however, and evaluation of the accuracy of the results in this range can only be attempted at the present time by comparison with experimental results.

Comparison With Existing Experimental Results for Supercritical Flows

The appeal to experiment to judge the quality of an approximate solution of the equations of compressible flow is nowhere a more uncertain procedure than in the range of Mach numbers somewhat greater than the critical in which the shock wave is situated upstream of the trailing edge. The principal reason is that the theoretical results are based on the assumption of an inviscid gas, whereas numerous experimental investigations (see, e.g., refs. 14 through 19) indicate that viscous effects associated with interaction of the shock wave and the boundary layer are frequently, if not invariably, of substantial magnitude in the general vicinity of the point where the shock wave meets the boundary layer. A resumé of some of the more prominent aspects of these phenomena is given in reference 1.

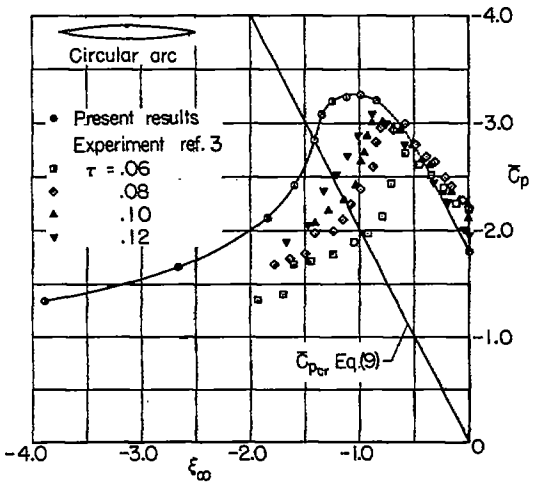

Sketch (7)

As a start toward a more specific discussion of the present results, consider the comparison shown in sketch (7) of the theoretical and experimental variations of $\bar{C}_p$ with ξ_∞ at the midpoint of symmetrical circular-arc airfoils. The circles joined by the solid line represent the calculated results for a thin airfoil of arbitrary thickness ratio. The other data points represent the experimental results from reference 3 for four airfoils having thickness ratios of 0.06, 0.08, 0.10, and 0.12 and should, according to the transonic similarity rule, define a single curve. Although the theoretical and experimental results are in reasonable agreement at Mach numbers near 1 and are qualitatively similar at all Mach numbers, it can be seen that substantial quantitative discrepancies exist for Mach numbers in the general vicinity of the critical. It is unlikely that these discrepancies at the midchord station can be attributed to shock-wave boundary-layer interaction. Examination of the results for the other airfoils of the present investigation reveals similar discrepancies when compared with the experimental data of Michel, Marchaud, and Le Gallo given in reference 4. Since the results for the circular-arc airfoil are typical of those for

all of the airfoils considered herein, most of the following discussion is concerned with closer examination of the results for this particular airfoil.

Experimental pressure distributions for supercritical flows past symmetrical circular-arc airfoils have been published not only in references 3 and 4, but also in references 14 and 15 by Liepmann, Ashkenas, and Cole, and in reference 16 by Wood and Gooderum. It should be noted, however, that the investigations reported in references 14 and 15 are concerned primarily with boundary-layer shock-wave interaction and the authors include statements in reference 14 casting doubt on the accuracy of the values indicated for the free-stream Mach number, a quantity of only secondary importance in their investigations. The variation of $\bar{C}_p$ with ξ_∞ at the midpoint of these airfoils is presented in sketch (m) in exactly the same manner as in sketch (l) so that the two sets of results should coincide. It can be seen that such coincidence of the results is again observed at Mach numbers near 1, but that there is wide scatter in the results for Mach numbers in the vicinity of the critical. It is interesting to observe in all these cases, as well as in others for Mach number 1 given in reference 2, that the experimental results for the thicker airfoils are generally in better agreement with the calculated results than those for the thinner airfoils. This trend is contrary to what might be expected if a major source of error were associated with the assumption of small disturbances in the establishment of the equations of transonic flow theory.

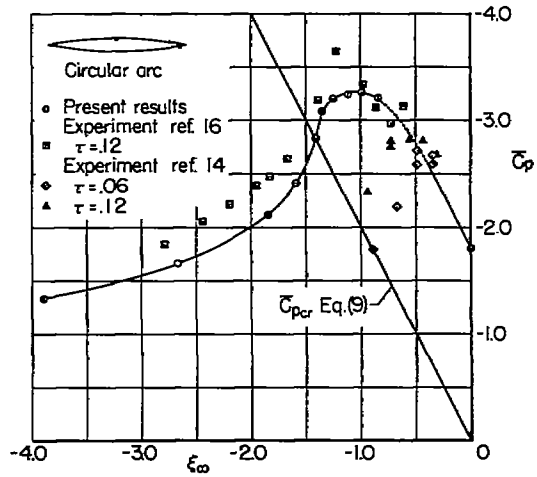

Sketch (m)

Inasmuch as the differences among the various sets of results exist at Mach numbers less than as well as greater than the critical, it is possible to explore the accuracy of the various results by comparison with the third-order approximation of Asaka to the solution of the complete equations of subsonic compressible flow theory. Since the latter theory includes terms disregarded in transonic flow theory and results for airfoils of different thickness ratios do not collapse perfectly onto a single line when plotted in terms of $\bar{C}_p$ and ξ_∞, the results are given in sketch (n) in terms of C_p and M_∞. In order to avoid confusion due to overlap, the intermediate thickness ratios, $\tau = 0.08$ and $\tau = 0.10$, have been omitted. It can be seen that none of the experimental results are in good agreement with the values indicated by higher order theory. Inasmuch as there is considerable evidence from various sources that higher order theory generally provides results that agree well with those found experimentally for Mach numbers up to the critical, it would appear that

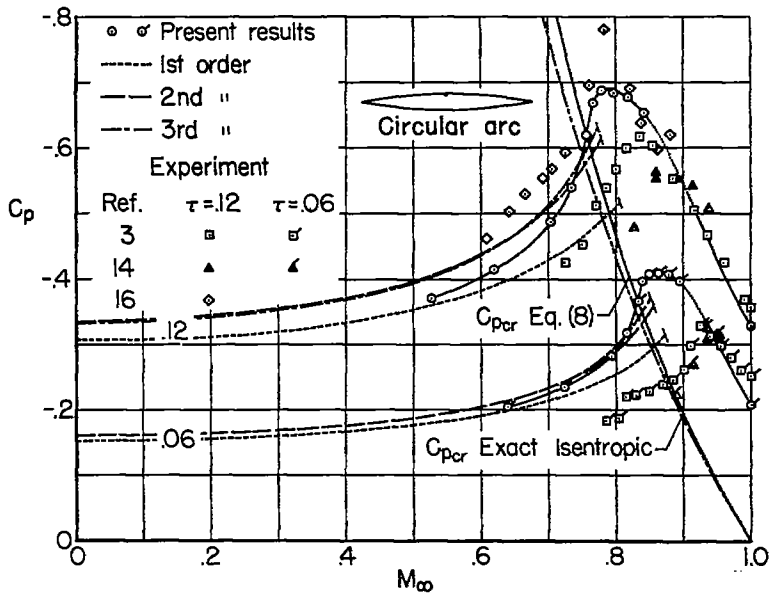

Sketch (n)

the source of the discrepancy should be sought in some facet of the experimental technique.

Some disagreement between theoretical and experimental pressure distributions, although generally of much smaller magnitude than that observed in sketches (ℓ) through (n), must always be anticipated to result from the presence of the boundary layer. The influence of this factor may be somewhat greater than usual in the experimental investigations of references 3 and 4 because the airfoil is not mounted in the middle of the tunnel as is customary, but is simulated by a bump on the tunnel wall, and is hence imbedded in the wall boundary layer. The authors of references 3 and 4 have considered this point, however, and included some evidence that indicates the experimental results on the 12-percent-thick circular-arc airfoil at a Mach number of 0.99 are substantially the same as those on a similar airfoil mounted in the middle of the tunnel and having a boundary layer artificially made turbulent. No corresponding information is presented for lower Mach numbers or for the thinner airfoils for which the relative effects of the boundary layer would be greater. Although it is recognized that the influence of the boundary layer on the pressure distribution is not the same for all Mach numbers, it is difficult to account for the small discrepancies between theory and experiment near Mach number 1 and the large discrepancies near the critical Mach number by boundary-layer effects alone. It appears, therefore, that some other factor might be supplying a substantial contribution to the observed discrepancies.

A source of uncertainty that is present in all wind-tunnel testing is associated with the finite dimensions of the test section. The study of wall interference and the determination of formulas for the calculation of corrections have consequently been the subject of numerous investigations (see, e.g., refs. 20 through 25). It is found, for airfoils and test sections of typical proportions, that the influence of the walls is generally small at low Mach numbers, but increases substantially as the Mach number increases toward and into the transonic range. Preliminary investigation reveals, moreover, that it appears plausible to attribute a substantial amount of the present discrepancies to this source.

In order to be more specific, consider the problem of transonic flow past a thin nonlifting airfoil of chord c and thickness ratio τ mounted in the center of a wind tunnel of height $2h$. The aerodynamic properties of this airfoil are to be compared with those of the same airfoil in an unbounded flow with free-stream velocity U_∞. It is considered that the apparent free-stream velocity in the wind tunnel, as determined from measurements of pressure at a point far upstream in the test section or in the plenum chamber of a ventilated wind tunnel, is not necessarily equal to U_∞, but is given by $U_\infty + u_\infty$ where u_∞ is much less than U_∞. The appropriate equations for the study of such flows are thus equations (4) through (6) together with the following relation for the pressure coefficient $C_{p_{WT}}$ on the airfoil in the wind tunnel

$$C_{p_{WT}} = -\frac{2(u-u_\infty)}{U_\infty} \tag{35}$$

and an additional boundary condition at $z = \pm h$ determined by the nature of the wall. This condition is $w = 0$ if the test section has solid walls, $u = u_\infty$ if the test section is an open jet, and a more complicated relation if the test section has porous or slotted walls. It is not necessary to be more specific about the boundary condition for the latter case at this point, since it is shown in references 21 and 22 that the influence of a ventilated wall is intermediate between that of a solid wall and an open jet.

The linearized theory of wind-tunnel wall interference follows directly from the equations enumerated above upon replacing the right-hand sides of equations (5) and (6) by zero. It is found, provided the dimensions of the section are large compared with those of the airfoil, that the net effect of the walls at subsonic Mach numbers is that the pressure p (not C_p) and local Mach number at the surface of the airfoil in the wind tunnel in a flow with apparent free-stream velocity $U_\infty + u_\infty$ is the same as at the surface of an identical airfoil in an unbounded flow with free-stream velocity U_∞. The quantity u_∞ is given by

$$\frac{u_\infty}{U_\infty} = C\frac{\tau}{(1-M_\infty^2)^{3/2}H^2} \tag{36}$$

where H represents h/c and C is a constant, the value of which depends on the nature of the walls of the test section; for example,

$$\left.\begin{aligned} C &= -\frac{\pi}{6}\frac{A_c}{tc} \qquad \text{solid walls} \\ C &= +\frac{\pi}{12}\frac{A_c}{tc} \qquad \text{open jet} \end{aligned}\right\} \tag{37}$$

where A_c is the area of the airfoil section. The influence of the tunnel walls on C_p follows directly upon combination of equations (35) and (36). It is

$$\Delta C_p = C_p - C_{p_{WT}} = -2\frac{u_\infty}{U_\infty} \tag{38}$$

Comparison with other results presented in this report is facilitated by rewriting equations (36) and (38) in terms of $\bar{C}_p$ and ξ_∞, thus

$$\Delta\xi_\infty = \xi_\infty - \xi_{\infty_{WT}} = -\frac{C}{(-\xi_\infty)^{3/2}\bar{H}^2} \tag{39}$$

$$\Delta\bar{C}_p = \bar{C}_p - \bar{C}_{p_{WT}} = 2\,\Delta\xi_\infty \tag{40}$$

where

$$\xi_{\infty_{WT}} = -\frac{1-M_\infty^2-ku_\infty}{(U_\infty k\tau)^{2/3}}, \qquad \bar{H} = (U_\infty k\tau)^{1/3}H$$

If the influence of the walls is examined for a family of airfoils of different thickness ratio and with the apparent Mach numbers in the wind tunnel selected so as to maintain a given ξ_∞, and thereby to secure similarity of transonic phenomena such as the critical Mach number, etc., it is evident from equations (39) and (40) that $|\Delta\xi_\infty|$ and $|\Delta\bar{C}_p|$ are inversely proportional to the square of $\bar{H}$. It follows immediately that $|\Delta\xi_\infty|$ and $|\Delta\bar{C}_p|$ diminish if either the height-chord ratio h/c of the tunnel or the thickness ratio τ of the airfoil is increased.

Added insight into the nature of the influence of the tunnel walls can be had by examining the curves given in sketch (o) showing the variation of $\bar{C}_p$ with ξ_∞ at the midpoint of a symmetrical circular-arc airfoil in an unbounded flow (or the variation of $\bar{C}_{p_{WT}}$ with $\xi_{\infty_{WT}}$ for infinite $\bar{H}$) together with the corresponding values for $\bar{C}_{p_{WT}}$ with $\xi_{\infty_{WT}}$ computed by use of equations (39) and (40) for the same airfoil mounted in either a closed wind tunnel or an open jet of such dimensions that $\bar{H}$ equals either 1 or $\sqrt{2}$. The value of unity for $\bar{H}$ corresponds, for instance, to that associated with a 6-percent-thick airfoil in a wind tunnel having a ratio of semiheight to chord h/c of 7/3 (the same as that for the experimental data shown in sketch (l)) at an effective free-stream Mach number M_∞ of approximately 0.75. Although the curves are continued to supercritical Mach numbers for which the use of linear theory to calculate the influence of the tunnel walls may be open to question, it is interesting to observe that the differences between the results for an unbounded flow and for an airfoil in an open jet are qualitatively similar to those that can be observed in sketch (l) between the theoretical results for an unbounded flow and the experimental results measured in a wind tunnel with slotted test section. The differences between the theoretical and experimental results are larger than indicated by the linear theory of wall interference, but quantitative agreement should perhaps not be expected since it is well known that substantial nonlinear effects occur at Mach numbers of the order of the critical and greater.

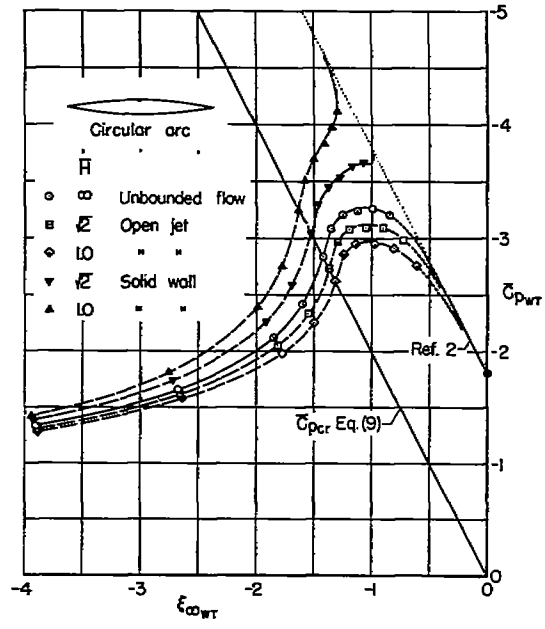

Sketch (o)

An interesting property of the linear theory for the influence of the tunnel walls is that there is a maximum value for $\xi_{\infty_{WT}}$, and hence the apparent free-stream Mach number, in a closed tunnel. This result is at least qualitatively consistent with the familiar property of choking of wind tunnels with solid walls. If the dimensions of the test section are sufficiently large compared with those of the airfoil, the values for $\bar{C}_{p_{WT}}$ associated with the maximum value for $\xi_{\infty_{WT}}$ are on the extension of a line $\bar{C}_p - 2\xi_\infty = \bar{C}_{p_{M_\infty=1}}$. Since $\bar{C}_p - 2\xi_\infty$ is equal to -2ξ, which is the reduced quantity associated with the local Mach number, this result indicates that the local Mach number distribution measured on an airfoil in a solid-wall tunnel of sufficiently great dimensions under choking conditions is the same as in an unbounded flow with free-stream Mach number 1. This conclusion is in complete accordance with the more

reliable theoretical results, based on nonlinear transonic flow theory, for flow past a wedge airfoil and a lifting flat plate (refs. 24 and 25), and with experimental results for an NACA 64A008 airfoil tested in several test sections of different sizes (ref. 26).

Linear theory indicates infinite corrections when $M_\infty = 1$ and must be replaced by a corresponding theory based on the nonlinear equations of transonic flow theory. This theory is not developed as far as the linear theory, but it is clear from similarity considerations that the functional form for the expression for $\overline{C}_{p_{WT}}$ for a family of affinely related airfoils in a wind tunnel is

$$\overline{C}_{p_{WT}} = f(\xi_\infty, \frac{x}{c}, \Delta\xi_\infty, \overline{H}) \tag{41}$$

plus additional parameters indicative of the porosity of the walls or of the geometry of the slots for wind tunnels with ventilated test sections.

If it is assumed that the local Mach number distribution measured on an airfoil in a wind tunnel is the same as that measured in an unbounded flow, in accordance with the indications of linear theory, equation (40) again applies together with an expression for $\Delta\xi_\infty$ that has the following form:

$$\Delta\xi_\infty = f(\xi_\infty, \overline{H}) \tag{42}$$

Equation (39), obtained from linear theory, is consistent with this functional expression and is, moreover, the precise relation that the solution of the nonlinear equations of transonic flow theory must approach as the free-stream Mach number tends toward zero. Although analysis of the influence of the walls based on consideration of $\Delta\overline{C}_p$ and $\Delta\xi_\infty$ as described above is similar to that successfully employed for low-speed flows, it may not be the best procedure to follow for Mach numbers near 1. The reason is that the corrections must inevitably become large at Mach numbers near 1 as a result of the fact that $\overline{C}_p - 2\xi_\infty$ is independent of ξ_∞ in this range.

Alternative procedures that lead to smaller corrections at Mach numbers near 1 are to consider $\Delta\overline{C}_p$ at $\xi_{\infty_{WT}} = \xi_\infty$, or to find $\Delta\xi_\infty$ so that $\overline{C}_{p_{WT}} = \overline{C}_p$ at some representative point on the airfoil. If the former point of view is adopted it follows from equation (41) that $\Delta\overline{C}_p$ is a function of ξ_∞ and $\overline{H}$. At Mach number 1, ξ_∞ is zero and $\Delta\overline{C}_p$ depends only on $\overline{H}$, thus

$$\Delta\overline{C}_{p_{\xi_\infty=0}} = f(\overline{H}) \tag{43}$$

If it is assumed that $|\Delta\bar{C}_p|$ decreases with increasing $\bar{H}$, as appears reasonable since $|\Delta\bar{C}_p|$ would be expected to be smaller if a given airfoil were tested in a large wind tunnel than in a small wind tunnel, it follows again that $|\Delta\bar{C}_p|$ is smaller for a thick airfoil than for a thin airfoil of affinely related geometry tested in a given wind tunnel.

Although the above discussion applies strictly only to families of affinely related airfoils, certain properties of the asymptotic solution for the flow at great distances from an airfoil at Mach number 1 suggest that the magnitude of $|\Delta\bar{C}_p|$ is greater for airfoils having maximum thickness far aft than for those having maximum thickness far forward. The reason is that it is not so much the thickness and chord of the complete airfoil that matters in the expressions for the asymptotic solution at Mach number 1, but the part of the thickness and chord that is more indicative of the portion of the airfoil that can influence the subsonic part of the flow field. This point has been discussed by Barish (ref. 27) who suggests the use of values of thickness t^* and chord c^* that are associated with the sonic point. This suggestion is based upon the observation that numerical calculations indicate the asymptotic flow fields of wedges and certain cusped-nosed airfoils are nearly independent of the details of the shape, provided t^* and c^* are fixed. It follows, to whatever extent this observation is generally true, that the relation corresponding to equation (43), but appropriate for nonaffinely, as well as affinely, related airfoils is of the following form:

$$\Delta\bar{C}_p{}^* = f(\bar{H}^*) \tag{44}$$

where

$$\Delta\bar{C}_p{}^* = \frac{[M_\infty{}^2(\gamma+1)]^{1/3}}{\tau^{*2/3}}\Delta C_p \ , \qquad \bar{H}^* = [M_\infty{}^2(\gamma+1)\tau^*]^{1/3}H^*$$

$$H^* = \frac{h}{c^*} \ , \qquad \tau^* = \frac{t^*}{c^*}$$

It is evident from inspection of sketches (l) and (m), as well as the more extensive set of results given in reference 2, that a substantial part of the discrepancies between the theoretical and experimental results for Mach number 1 possesses properties consistent with those described above for the influence of the wind-tunnel walls. This correspondence prompts the presentation of sketch (p) which shows the variation of $\Delta\bar{C}_p{}^*$ with $\bar{H}^*$ at free-stream Mach number 1 at the point on the airfoil surface at which sonic velocity occurs in free air. The values for $\Delta\bar{C}_p{}^*$ were computed using the theoretical values given in

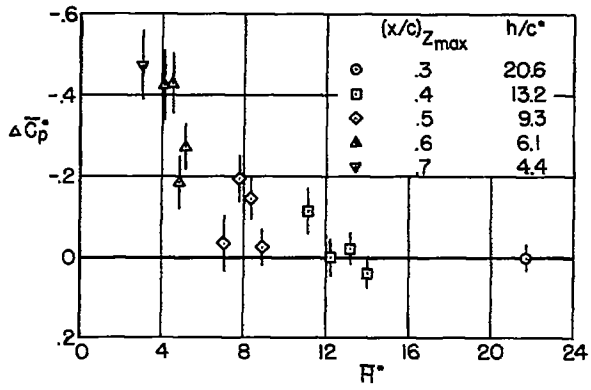

Sketch (p)

reference 2 for $\bar{C}_p$ and the experimental values given in references 3 and 4 for $\bar{C}_{p_{WT}}$. The location of the sonic point and hence the values of t* and c* are thus determined from the theoretical solution. Although the general procedure may be open to some question and scatter is inevitably large since $\Delta\bar{C}_p^*$ is basically a small difference of larger quantities (some idea of the uncertainty of the values for $\Delta\bar{C}_p^*$ can be gained by consideration of the vertical line through each data point indicating the range of values associated with an arbitrary change of 1 percent in the local Mach number), the results display a reasonably well-defined trend consistent with the ideas that $\Delta\bar{C}_p^*$ does depend on $\bar{H}^*$ and that $|\Delta\bar{C}_p^*|$ diminishes with increasing $\bar{H}^*$.

Pressure Drag

Once the pressure distribution is known for a given airfoil, the pressure drag d can be calculated by use of the following relation:

$$c_d = \frac{d}{(\rho_\infty/2)U_\infty^2 c} = \frac{2}{c}\int_0^c C_p \frac{dZ}{dx}\,dx \tag{45}$$

It is convenient at this point to introduce a reduced drag coefficient $\bar{c}_d$ defined in terms of reduced quantities, thus

$$\bar{c}_d = \frac{2}{c}\int_0^c \bar{C}_p \frac{d(\bar{Z}/\bar{\tau})}{d\bar{x}}\,d\bar{x} \tag{46}$$

It is clear from the definitions of $\bar{C}_p$, $\bar{\tau}$, $\bar{Z}$, and $\bar{x}$ that the relation between c_d and $\bar{c}_d$ is

$$\bar{c}_d = \frac{[M_\infty^2(\gamma+1)]^{1/3}}{\tau^{5/3}} c_d$$

The variation of $\bar{c}_d$ with ξ_∞ has been computed for the symmetrical circular-arc airfoil. The results are summarized below and illustrated graphically in sketch (q). Three classes of results are included in this

ξ_∞	$\bar{c}_d$
-1.42	0
-1.35	.00
-1.25	.12
-1.12	.65
-.985	1.99
-.838	4.97

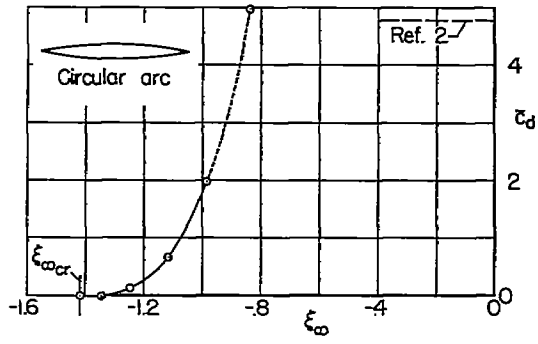

Sketch (q)

sketch and are distinguished by the type of line. The solid portion of the curve represents the values for Mach numbers up to that at which the shock wave has moved to 0.9 chord and is determined by direct application of the pressure-distribution results for $\xi_\infty \leq -0.985$ given in table I and summarized in figure 3. The continuation of the curve to a value for ξ_∞ of -0.838 is determined in a similar manner, but is indicated by a dashed line because the calculated pressure distribution is inaccurate in the vicinity of the trailing edge when the shock wave is at the trailing edge. The portion of the curve marked by long dashes represents the value 4.77 given in reference 2 for Mach numbers near unity. In all cases, the integrations required to determine the drag were evaluated using Simpson's rule. Very fine intervals were used near the leading and trailing edges and the contributions of the regions in the immediate vicinity of the leading- and trailing-edge singularities were evaluated analytically in order to achieve the desired degree of accuracy.

It can be seen by examination of the results shown in sketch (q) that $\bar{c}_d$ is zero for $\xi_\infty < -1.42$ (corresponding to the critical Mach number). It remains nearly zero as ξ_∞ increases to -1.35, and then rises rapidly with further increases of ξ_∞. The increase in drag is associated principally with the rearward movement of the shock wave across the chord and terminates abruptly when the shock reaches the trailing edge at $\xi_\infty = -0.838$. Although no values for drag are given, it is evident from inspection of the variation of $\bar{c}_p$ with ξ_∞ indicated in figure 8 that further increases in ξ_∞ result in only small changes in $\bar{c}_d$, and that finally, at a value of ξ_∞ somewhat less than zero, $\bar{c}_d$ becomes invariant with further changes in ξ_∞.

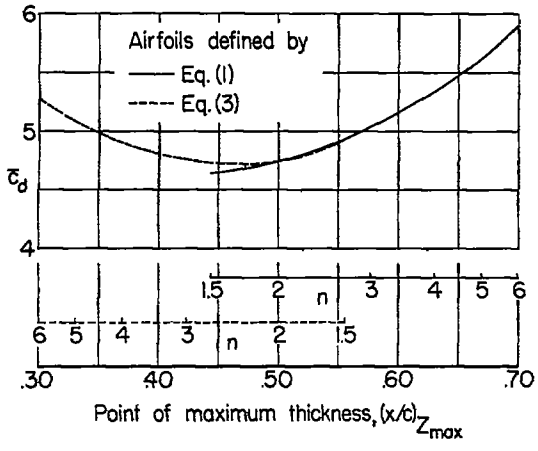

Sketch (r)

The values for the drag of the other airfoils considered in the present investigation have been calculated only for Mach numbers near unity. These results, given originally in reference 2, are summarized in sketch (r) together with the corresponding results for related airfoils defined by equations (1) and (3) upon insertion of values for n ranging from 1.50 to 6.05.

There are no experimental results for the pressure drag of symmetrical circular-arc airfoils that are of sufficient reliability to provide a clear evaluation of the accuracy of the calculated results shown in sketch (q). The most extensive results are those given by Michel, Marchaud, and Le Gallo in reference 3 for four airfoils of different thickness ratio. These results were obtained by integration of the measured pressure distributions and suffer in quality, not only as a result of the factors discussed in the preceding section of this report, but also because of lack of sufficient pressure-distribution data for points near the leading and trailing edges. The results of Michel, Marchaud, and Le Gallo are presented, nevertheless, in sketch (s) together with the theoretical results from sketch (q). Also included in sketch (s) are the theoretical values for $\bar{c}_d$ for purely supersonic flow. The latter results are from reference 2 and were calculated by integration of pressure distributions obtained by application of a simplified form of simple wave theory that is consistent with the equations of transonic flow theory.

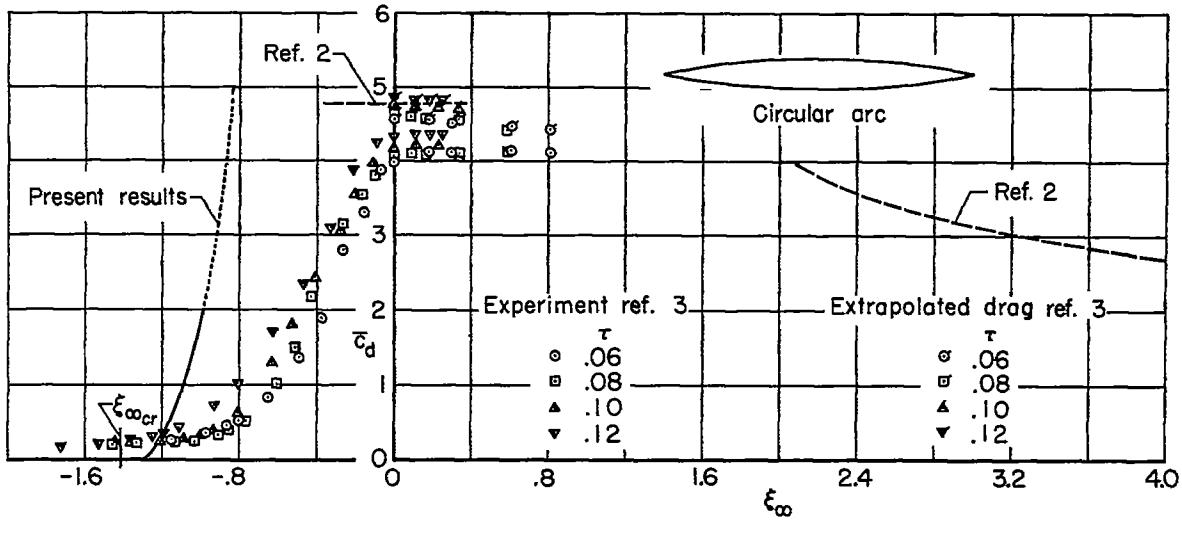

Sketch (s)

Examination of the results shown in sketch (s) reveals that the theoretical and experimental variations of $\bar{c}_d$ with ξ_∞ exhibit the same general trends but are quantitatively quite different. Part of the difference is undoubtedly associated with boundary-layer shock-wave interaction. As discussed at greater length in reference 1, this phenomenon can have considerable influence on the drag, but is disregarded completely in the basic formulation of transonic flow theory. From the standpoint of drag, one of the principal effects of shock-wave boundary-layer interaction appears to be that the shock wave is moved to a more forward location along the chord. The pressures on the rear part of the airfoil are increased as a result and a substantial reduction in drag follows. These effects are largest at Mach numbers somewhat greater than the critical, but persist to a lesser degree for sonic and even purely supersonic flows. Because this phenomenon depends on Reynolds number and may be of greatly diminished importance at full-scale conditions, Michel, Marchaud, and Le Gallo introduced in the discussion of their experimental results for free-stream Mach numbers equal to or greater than unity the concept of "extrapolated drag" to represent the drag that would occur in the absence of separation. This quantity is calculated by consideration of a pressure distribution that differs from the experimental pressure distribution in the vicinity of the trailing edge as a result of the replacement of the pressures actually measured by those obtained by extrapolation of the trends indicated at stations upstream of the separation point. Accordingly, the values for extrapolated drag given by Michel, Marchaud, and Le Gallo are also shown in sketch (s). As might be expected, the theoretical values for drag are in better agreement with the values for extrapolated drag than with those obtained directly from the actual measurements.

Another part of the difference between the theoretical and experimental values for drag is associated with the higher critical Mach numbers displayed by the experimental results in sketch (s) and is probably to be attributed to the influence of the wind-tunnel walls. Some idea of the magnitude of these effects can be gained by examination of sketch (t), which shows the variation of $\bar{c}_d$ with ξ_∞ for a symmetrical circular-arc airfoil in an unbounded flow (or the variation of $\bar{c}_{d_{WT}}$ with $\xi_{\infty_{WT}}$ for infinite $\bar{H}$)

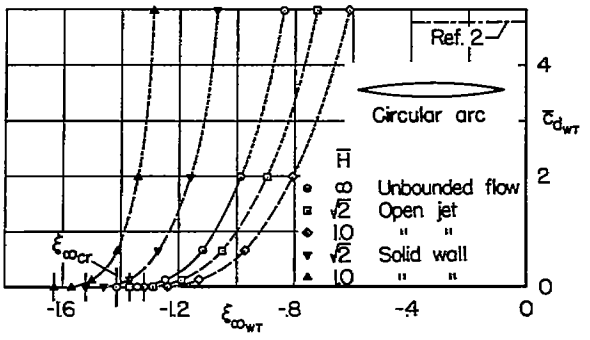

Sketch (t)

together with the corresponding values for $\bar{c}_{d_{WT}}$ and $\xi_{\infty_{WT}}$ computed by use of equations (39) and (40) for the same airfoil mounted in either a closed wind tunnel or open jet of such dimensions that $\bar{H}$ equals either 1 or $\sqrt{2}$. These values of $\bar{H}$ are the same as considered in sketch (o). Sketch (t) illustrates that the effect of the finite dimensions of the test section is such that the values for $\bar{c}_{d_{WT}}$ remain equal to the

corresponding values for an airfoil in an unbounded flow, although experienced at different values of ξ_∞, or Mach number. As a result, significant effects of the walls are observed in the variation of $\bar{c}_{d_{WT}}$ with $\xi_{\infty_{WT}}$ at Mach numbers somewhat greater than the critical. All such differences disappear at Mach numbers near unity in an open jet or near choking in a solid-wall wind tunnel, however, since $\bar{c}_d$ is independent of ξ_∞ in this range. Examination of sketch (t) reveals again that the differences between the results for an unbounded flow and for an airfoil in an open jet are qualitatively similar to those that can be observed in sketch (s) between the theoretical results for an unbounded flow and the experimental results measured in a wind tunnel with slotted test section.

Ames Aeronautical Laboratory
National Advisory Committee for Aeronautics
Moffett Field, Calif., Oct. 22, 1957

REFERENCES

1. Spreiter, John R., and Alksne, Alberta: Theoretical Prediction of Pressure Distributions on Nonlifting Airfoils at High Subsonic Speeds. NACA Rep. 1217, 1955. (Supersedes NACA TN 3096)

2. Spreiter, John R., and Alksne, Alberta Y.: Thin Airfoil Theory Based on Approximate Solution of the Transonic Flow Equation. NACA TN 3970, 1957.

3. Michel, R., Marchaud, F., and Le Gallo, J.: Etude des écoulements transsoniques autour des profils lenticulaires, a incidence nulle. O.N.E.R.A. Pub. No. 65, 1953.

4. Michel, R., Marchaud, F., and Le Gallo, J.: Influence de la position du maitre-couple sur les écoulements transsoniques autour de profils a pointes. O.N.E.R.A. Pub. No. 72, 1954.

5. Heaslet, Max. A., and Spreiter, John R.: Three-Dimensional Transonic Flow Theory Applied to Slender Wings and Bodies. NACA Rep. 1318, 1957. (Supersedes NACA TN 3717)

6. Oswatitsch, K.: Die Geschwindigkeitsverteilung bei lokalen Überschallgebieten an flachen Profilen. Z.a.M.M., Bd. 30, Nr. 1/2, Jan./Feb. 1950, S. 17-24.

7. Oswatitsch, Klaus: Die Geschwindigkeitsverteilung an symmetrischen Profilen beim Auftreten lokaler Überschallgebiete. Acta Physica Austriaca, Bd. 4, Nr. 2/3, Dec. 1950, S. 228-271.

8. Humphreys, Milton D.: Pressure Pulsations on Rigid Airfoils at Transonic Speeds. NACA RM L51I12, 1951.

9. Van Dyke, Milton D.: Second-Order Subsonic Airfoil Theory Including Edge Effects. NACA Rep. 1274, 1956.

10. Hantzsche, W., and Wendt, H.: Der Kompressibilitätseinfluss für dünne wenig gekrümmte Profile bei Unterschallgeschwindigkeit. Z.a.M.M., Bd. 22, Nr. 2, Apr. 1952, pp. 72-86.

11. Asaka, Saburô: On the Velocity Distribution Over the Surface of a Symmetrical Aerofoil at High Speeds, II. National Science Report of the Ochanomizu University, vol. 5, no. 1, 1954, pp. 59-78.

12. Asaka, Saburô: Application of the Thin-Wing-Expansion Method to the Flow of a Compressible Fluid Past a Symmetrical Circular Arc Aerofoil. Jour. Phy. Soc. Japan, vol. 10, no. 6, June 1955, pp. 482-492.

13. Asaka, Saburô: Errata: Application of the Thin-Wing-Expansion Method to the Flow of a Compressible Fluid Past a Symmetrical Circular Arc Aerofoil. Jour. Phy. Soc. Japan, vol. 10, no. 7, July 1955, p. 593.

14. Liepmann, Hans Wolfgang, Ashkenas, Harry, and Cole, Julian D.: Experiments in Transonic Flow. Tech. Rep. No. 5667, Air Materiel Command, U. S. Air Force, Feb. 9, 1948.

15. Liepmann, Hans Wolfgang: The Interaction Between Boundary Layer and Shock Waves in Transonic Flow. Jour. Aero. Sci., vol. 13, no. 12, Dec. 1946, pp. 623-637.

16. Wood, George P., and Gooderum, Paul B.: Investigation With an Interferometer of the Flow Around a Circular-Arc Airfoil at Mach Numbers Between 0.6 and 0.9. NACA TN 2801, 1952.

17. Ackeret, J., Feldmann, F., and Rott, N.: Untersuchungen an Verdichtungsstössen und Grenzschichten in schnell bewegten Gasen. Mitteilungen aus dem Institut für Aerodynamik, Zurich, Nr. 10, 1946. (Also available as NACA TM 1113, 1947)

18. Harrin, Eziaslav N.: A Flight Investigation of the Effect of Shape and Thickness of the Boundary Layer on the Pressure Distribution in the Presence of Shock. NACA TN 2765, 1952.

19. Holder, D. W., Pearcey, H. H., and Gadd, G. E.: The Interaction Between Shock Waves and Boundary Layers, with a note on "The Effects of the Interaction on the Performance of Supersonic Intakes," by J. Seddon. C. P. No. 180, British A.R.C., 1955.

20. Allen, H. Julian, and Vincenti, Walter G.: Wall Interference in a Two-Dimensional-Flow Wind Tunnel, With Consideration of the Effect of Compressibility. NACA Rep. 782, 1944.

21. Baldwin, Barrett S., Jr., Turner, John B., and Knechtel, Earl D.: Wall Interference in Wind Tunnels With Slotted and Porous Boundaries at Subsonic Speeds. NACA TN 3176, 1954. (Supersedes NACA RM A53E29)

22. Maeder, Paul F., and Wood, Albert D.: Transonic Wind Tunnel Test Sections. Z.a.M.P., vol. 7, no. 3, 1956, pp. 177-212. (Also pub. as OSR TN-55-213)

23. Berndt, Sune B.: Theoretical Aspects of the Calibration of Transonic Test Sections. Flygtekniska Försöksanstalten Report 74, 1957. (Supersedes FFA Rapp. AE-400)

24. Marschner, Bernard W.: The Flow Over a Body in a Choked Wind Tunnel and in a Sonic Free Jet. Jour. Aero. Sci., vol. 23, no. 4, Apr. 1956, pp. 368-376.

25. Guderley, K. Gottfried: The Flat Plate with an Angle of Attack in a Choked Wind Tunnel. Jour. Aero. Sci., vol. 22, no. 12, Dec. 1956, pp. 844-866.

26. Larson, P. O., and Sörensén, H.: Bestämning au Tryckfördelningen på en Två-Dimensionell Vinge vid Olika Blokeringsmachtal. Flygtekniska Försöksanstalten Rapport SE-52.

27. Barish, David T.: Interim Report on a Study of Mach One Wind Tunnels. WADC Tech. Rep. 52-88, Apr. 1952.

TABLE I.- CALCULATED PRESSURE DISTRIBUTIONS

(a) $(x/c)_{z_{max}} = 0.30$

π_D

z_m \ x/c	0.025	0.05	0.10	0.15	0.20	0.25	0.30	0.35	0.40	0.45	0.50	0.55	0.60	0.65	0.70	0.75	0.80	0.85	0.90	0.95	0.975
-4.64	0.72	-0.21	-1.18	-1.58	-1.67	-1.62	-1.49	-1.33	-1.15	-0.98	-0.82	-0.66	-0.53	-0.41	-0.28	-0.17	-0.06	0.07	0.23	0.43	0.59
-2.23	1.05	-.14	-1.67	-2.44	-2.62	-2.55	-2.30	-2.02	-1.73	-1.45	-1.19	-.95	-.74	-.55	-.38	-.20	-.04	.13	.31	.58	.83
-1.84	1.16	-.08	-1.85	-2.80	-3.11	-3.05	-2.68	-2.29	-1.95	-1.62	-1.32	-1.04	-.80	-.59	-.39	-.21	-.03	.14	.36	.66	.90
-1.72	1.20	-.06	-1.88	-2.90	-3.36	-3.32	-2.84	-2.39	-2.00	-1.65	-1.35	-1.07	-.82	-.60	-.40	-.21	-.02	.17	.38	.68	.92
-1.62	1.26	-.03	-1.88	-2.96	-3.51	-3.83	-3.83 -2.64	-2.40	-2.03	-1.68	-1.36	-1.06	-.83	-.58	-.39	-.19	0	.13	.38	.70	.95
-1.47	1.35	.09	-1.81	-3.01	-3.64	-4.06	-4.33	-4.52	-4.42 -1.47	-1.40	-1.20	-.95	-.76	-.54	-.34	-.13	.06	.24	.43	.77	1.01
-1.37	1.45	.26	-1.71	-2.95	-3.61	-4.06	-4.39	-4.62	-4.77	-4.85	-4.87 -.62	-.64	-.49	-.33	-.17	0	.16	.33	.54	.87	1.09
-1.31	1.52	.26	-1.64	-2.88	-3.58	-4.03	-4.38	-4.64	-4.81	-4.91	-4.97	-5.02	-5.07 -.16	-.10	.01	.16	.31	.47	.64	.95	1.18
-1.26	1.57	.35	-1.58	-2.89	-3.55	-3.99	-4.32	-4.57	-4.74	-4.85	-4.95	-5.03	-5.09	-5.15	-5.20 .15	.27	.40	.54	.72	1.02	1.25
-1.24	1.59	.34	-1.54	-2.85	-3.49	-3.92	-4.27	-4.52	-4.69	-4.81	-4.90	-4.97	-5.04	-5.12	-5.20	-5.29	-5.42 .45	.58	.79	1.08	1.27
-1.24	1.59	.34	-1.54	-2.82	-3.52	-3.96	-4.27	-4.54	-4.71	-4.82	-4.91	-4.99	-5.07	-5.15	-5.22	-5.31	-5.42	-5.56	-5.74 .77	1.05	1.28
-1.24	1.59	.34	-1.53	-2.83	-3.52	-3.95	-4.26	-4.51	-4.69	-4.80	-4.88	-4.95	-5.04	-5.11	-5.20	-5.30	-5.40	-5.54	-5.72	-6.02	-6.23

(b) $(x/c)_{z_{max}} = 0.40$

-4.64	.86	.21	-.50	-.88	-1.13	-1.27	-1.34	-1.34	-1.30	-1.23	-1.13	-1.02	-.89	-.75	-.60	-.44	-.26	-.06	.18	.47	.74
-2.23	1.19	.34	-.64	-1.26	-1.67	-1.93	-2.05	-2.06	-2.00	-1.88	-1.72	-1.52	-1.31	-1.08	-.85	-.59	-.34	-.05	.25	.67	1.01
-1.84	1.29	.41	-.68	-1.36	-1.85	-2.17	-2.31	-2.34	-2.28	-2.13	-1.92	-1.70	-1.46	-1.19	-.91	-.63	-.33	-.01	.32	.74	1.09
-1.59	1.36	.46	-.68	-1.43	-2.02	-2.45	-2.68	-2.75	-2.62	-2.41	-2.16	-1.87	-1.57	-1.27	-.96	-.66	-.33	-.02	.35	.79	1.15
-1.50	1.40	.51	-.66	-1.44	-2.07	-2.58	-2.92	-2.97	-2.76	-2.50	-2.23	-1.95	-1.62	-1.30	-.96	-.65	-.34	-.01	.35	.81	1.18
-1.47	1.41	.50	-.65	-1.44	-2.10	-2.60	-2.96	-3.19	-3.29 -2.57	-2.97	-2.26	-1.95	-1.65	-1.34	-.99	-.66	-.33	-.01	.36	.82	1.19
-1.36	1.47	.56	-.60	-1.42	-2.08	-2.63	-3.07	-3.42	-3.64	-3.74	-3.63 -1.81	-1.80	-1.56	-1.26	-.94	-.62	-.30	.04	.42	.87	1.23
-1.26	1.53	.63	-.54	-1.36	-2.04	-2.61	-3.05	-3.39	-3.67	-3.90	-4.08	-4.17	-4.13 -.92	-.96	-.72	-.48	-.20	.13	.50	.94	1.31
-1.16	1.61	.71	-.46	-1.31	-2.00	-2.55	-3.00	-3.39	-3.68	-3.94	-4.14	-4.32	-4.43	-4.53	-4.50 -.15	-.12	.08	.33	.69	1.07	1.43
-1.08	1.68	.79	-.38	-1.23	-1.91	-2.47	-2.93	-3.32	-3.67	-3.91	-4.13	-4.32	-4.47	-4.60	-4.72	-4.82	-4.86 .54	.63	.87	1.25	1.58
-1.03	1.73	.85	-.31	-1.16	-1.82	-2.35	-2.88	-3.29	-3.62	-3.88	-4.11	-4.31	-4.45	-4.60	-4.73	-4.85	-4.97	-5.08	-5.23 1.12	1.43	1.72
-.995	1.76	.89	-.26	-1.14	-1.81	-2.35	-2.83	-3.26	-3.57	-3.82	-4.06	-4.24	-4.40	-4.53	-4.67	-4.78	-4.90	-5.03	-5.21	-5.50	-5.73

TABLE I.- CALCULATED PRESSURE DISTRIBUTIONS - Concluded

(c) $(x/c)_{z_{max}} = 0.50$																					
	$\bar{c}_p$																				
β_{∞} \ x/a	0.025	0.05	0.10	0.15	0.20	0.25	0.30	0.35	0.40	0.45	0.50	0.55	0.60	0.65	0.70	0.75	0.80	0.85	0.90	0.95	0.975
-3.90	.92	.43	-.15	-.50	-.76	-.94	-1.09	-1.20	-1.28	-1.32	-1.33	-1.32	-1.28	-1.20	-1.09	-.94	-.76	-.50	-.15	.43	.92
-2.67	1.07	.51	-.14	-.59	-.90	-1.15	-1.34	-1.49	-1.58	-1.64	-1.66	-1.64	-1.58	-1.49	-1.34	-1.15	-.90	-.59	-.14	.51	1.07
-1.84	1.24	.63	-.13	-.67	-1.08	-1.40	-1.65	-1.86	-1.99	-2.09	-2.12	-2.09	-1.99	-1.86	-1.65	-1.40	-1.08	-.67	-.13	.63	1.24
-1.59	1.31	.68	-.12	-.69	-1.12	-1.50	-1.81	-2.06	-2.25	-2.37	-2.42	-2.37	-2.25	-2.06	-1.81	-1.50	-1.12	-.69	-.12	.68	1.31
-1.42	1.37	.73	-.08	-.69	-1.17	-1.57	-1.94	-2.25	-2.50	-2.70	-2.83	-2.70	-2.50	-2.25	-1.94	-1.57	-1.17	-.69	-.08	.73	1.37
-1.35	1.39	.76	-.07	-.68	-1.18	-1.58	-1.97	-2.29	-2.59	-2.86	-3.08	-3.22	-3.13 -2.25	-2.18	-1.93	-1.57	-1.18	-.68	-.07	.76	1.39
-1.25	1.44	.81	-.03	-.65	-1.15	-1.57	-1.95	-2.30	-2.64	-2.94	-3.20	-3.43	-3.63	-3.75	-3.73 -1.25	-1.37	-1.04	-.59	.02	.83	1.46
-1.12	1.52	.88	.03	-.60	-1.11	-1.54	-1.93	-2.31	-2.64	-2.96	-3.24	-3.53	-3.77	-4.01	-4.20	-4.36	-4.37 -.10	-.18	.15	1.02	1.61
-.985	1.60	.98	.12	-.51	-1.02	-1.48	-1.89	-2.26	-2.63	-2.96	-3.27	-3.55	-3.83	-4.11	-4.37	-4.62	-4.84	-5.05	-5.23 1.29	1.48	1.95
-.838	1.69	1.09	.20	-.39	-.86	-1.34	-1.78	-2.18	-2.55	-2.88	-3.21	-3.52	-3.81	-4.10	-4.39	-4.69	-4.96	-5.26	-5.58	-5.99	-6.23
(d) $(x/a)_{z_{max}} = 0.60$																					
-4.64	.74	.47	.18	-.06	-.26	-.44	-.60	-.75	-.89	-1.02	-1.13	-1.23	-1.30	-1.34	-1.34	-1.27	-1.13	-.88	-.50	.21	.86
-2.23	1.01	.67	.25	-.05	-.34	-.59	-.85	-1.08	-1.31	-1.52	-1.72	-1.88	-2.00	-2.06	-2.05	-1.93	-1.67	-1.26	-.64	.34	1.19
-1.84	1.09	.74	.32	-.01	-.33	-.63	-.91	-1.19	-1.46	-1.70	-1.92	-2.13	-2.28	-2.34	-2.31	-2.17	-1.85	-1.36	-.68	.41	1.29
-1.59	1.15	.79	.35	-.02	-.33	-.66	-.96	-1.27	-1.57	-1.87	-2.16	-2.41	-2.62	-2.75	-2.68	-2.45	-2.02	-1.43	-.68	.46	1.36
-1.50	1.18	.81	.35	-.01	-.34	-.65	-.96	-1.30	-1.62	-1.95	-2.23	-2.50	-2.76	-2.97	-2.92	-2.58	-2.07	-1.44	-.66	.51	1.40
-1.46	1.19	.82	.36	0	-.35	-.66	-.98	-1.30	-1.63	-1.95	-2.26	-2.57	-2.89	-3.15	-3.04 -2.78	-2.62	-2.10	-1.45	-.64	.51	1.41
-1.32	1.24	.87	.41	.03	-.32	-.64	-.98	-1.31	-1.64	-1.98	-2.37	-2.72	-3.04	-3.34	-3.64	-3.90	-3.90 -1.37	-1.29	-.56	.61	1.51
-1.11	1.33	.97	.51	.12	-.23	-.57	-.93	-1.27	-1.61	-1.97	-2.40	-2.80	-3.20	-3.59	-4.00	-4.39	-4.80	-5.17	-5.31 .87	1.15	1.85
-.883	1.45	1.09	.63	.24	-.12	-.46	-.82	-1.18	-1.56	-1.96	-2.33	-2.72	-3.14	-3.58	-4.02	-4.47	-4.98	-5.50	-6.07	-6.67	-7.02
(e) $(x/c)_{z_{max}} = 0.70$																					
-4.64	.59	.43	.23	.07	-.06	-.17	-.28	-.41	-.53	-.66	-.82	-.98	-1.15	-1.33	-1.49	-1.62	-1.67	-1.58	-1.18	-.21	.72
-2.23	.83	.58	.31	.13	-.04	-.20	-.38	-.55	-.74	-.95	-1.19	-1.45	-1.73	-2.02	-2.30	-2.55	-2.62	-2.44	-1.67	-.14	1.05
-1.84	.90	.66	.36	.14	-.03	-.21	-.39	-.59	-.80	-1.04	-1.32	-1.62	-1.95	-2.29	-2.68	-3.05	-3.11	-2.80	-1.85	-.08	1.16
-1.72	.92	.68	.38	.17	-.02	-.21	-.40	-.60	-.82	-1.07	-1.35	-1.65	-2.00	-2.39	-2.84	-3.32	-3.36	-2.90	-1.88	-.06	1.20
-1.69	.94	.68	.38	.17	-.03	-.20	-.39	-.60	-.82	-1.08	-1.35	-1.67	-2.03	-2.44	-2.88	-3.39	-3.60 -3.17	-2.97	-1.87	-.05	1.22
-1.44	1.00	.73	.43	.21	.01	-.19	-.40	-.62	-.82	-1.09	-1.41	-1.74	-2.13	-2.56	-3.04	-3.63	-4.31	-5.00	-5.23 -.53	-.07	1.47
-1.21	1.08	.84	.49	.29	.06	-.14	-.34	-.56	-.80	-1.07	-1.39	-1.75	-2.17	-2.65	-3.21	-3.84	-4.55	-5.33	-6.17	-6.68 1.84	2.17
-.984	1.16	.91	.59	.35	.13	-.07	-.27	-.49	-.74	-1.04	-1.38	-1.75	-2.17	-2.67	-3.24	-3.90	-4.66	-5.56	-6.58	-7.76	-8.40

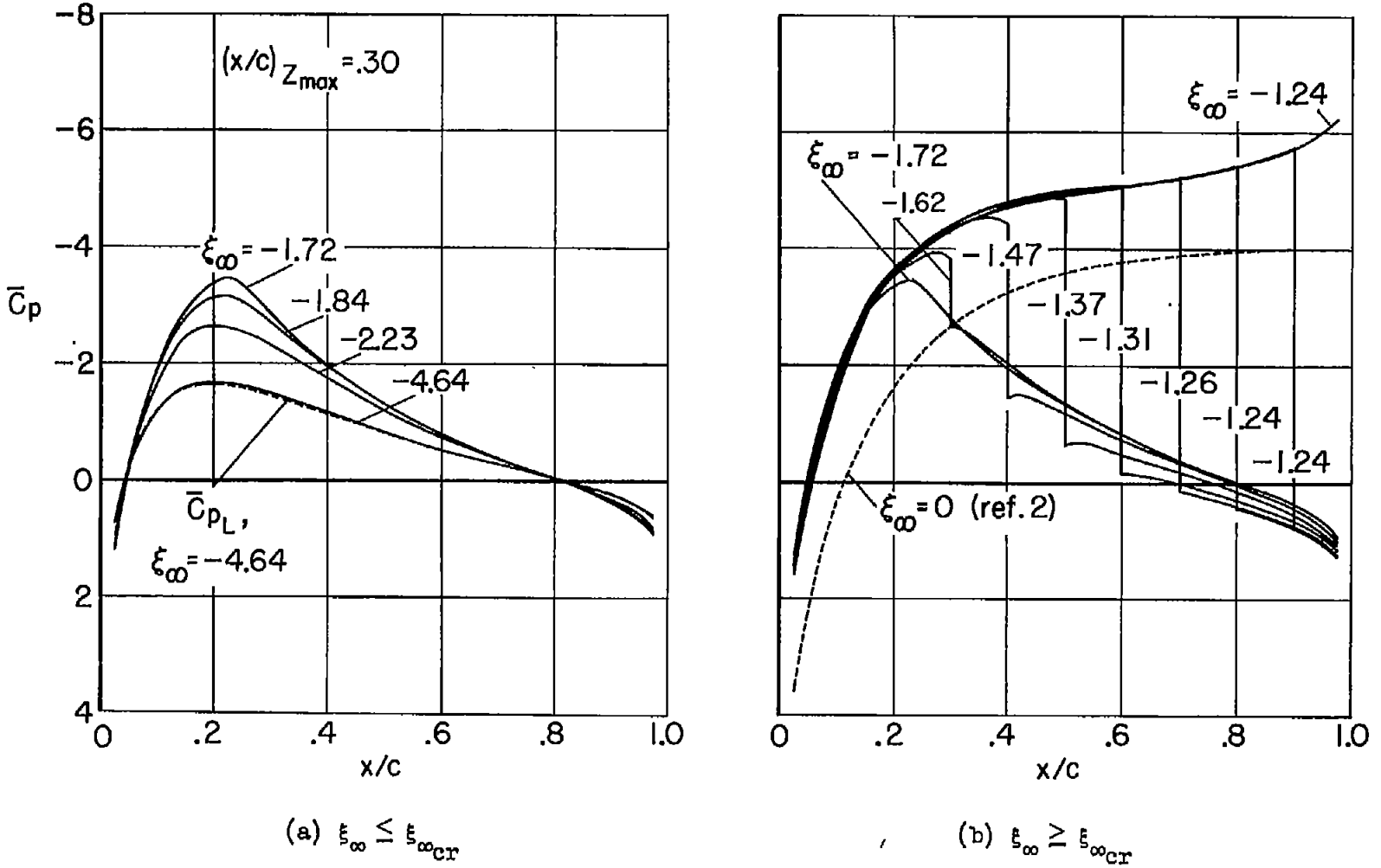

(a) $\xi_\infty \leq \xi_{\infty_{cr}}$ (b) $\xi_\infty \geq \xi_{\infty_{cr}}$

Figure 1.- Theoretical pressure distributions on an airfoil with maximum thickness at 30-percent chord.

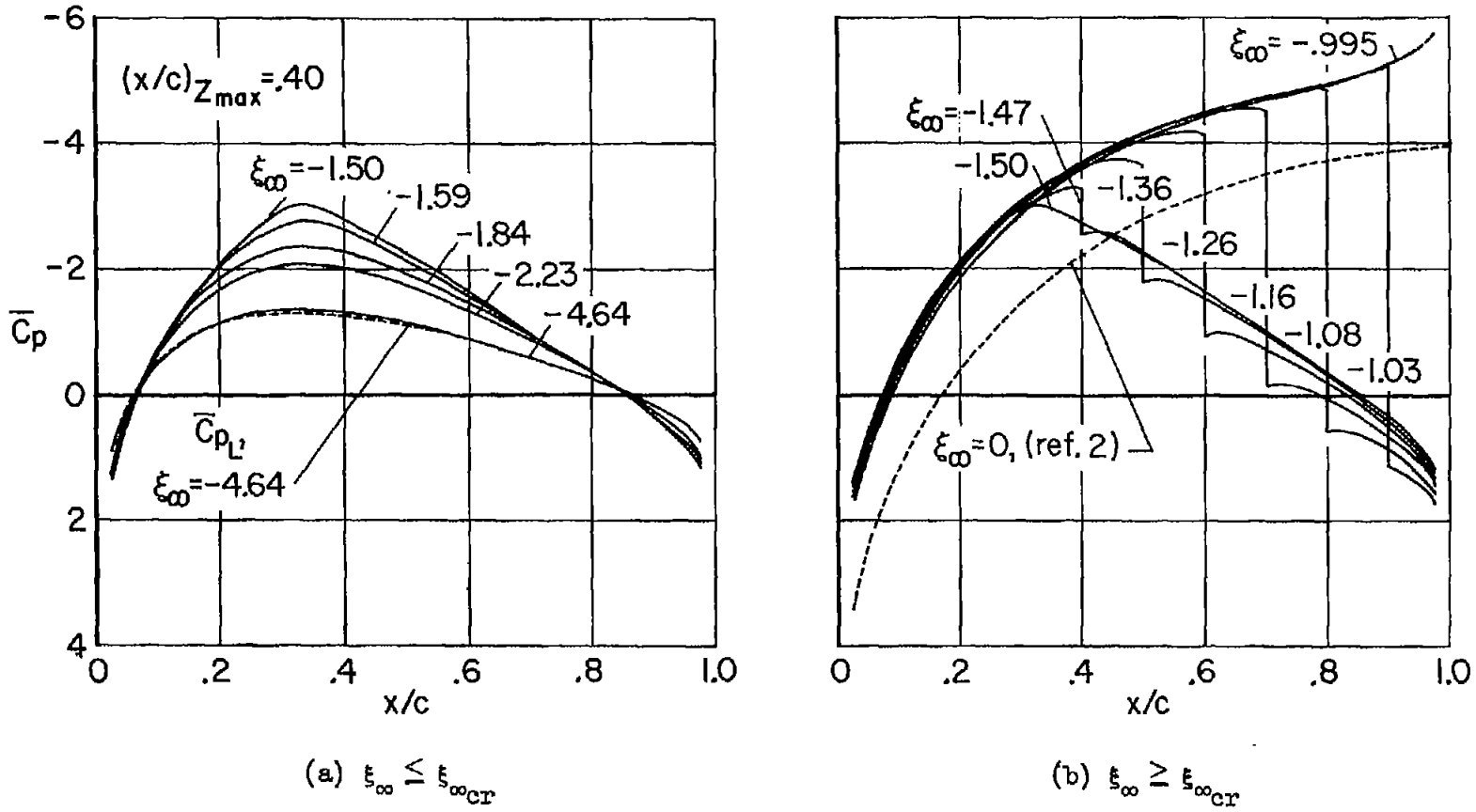

Figure 2.- Theoretical pressure distributions on an airfoil with maximum thickness at 40-percent chord.

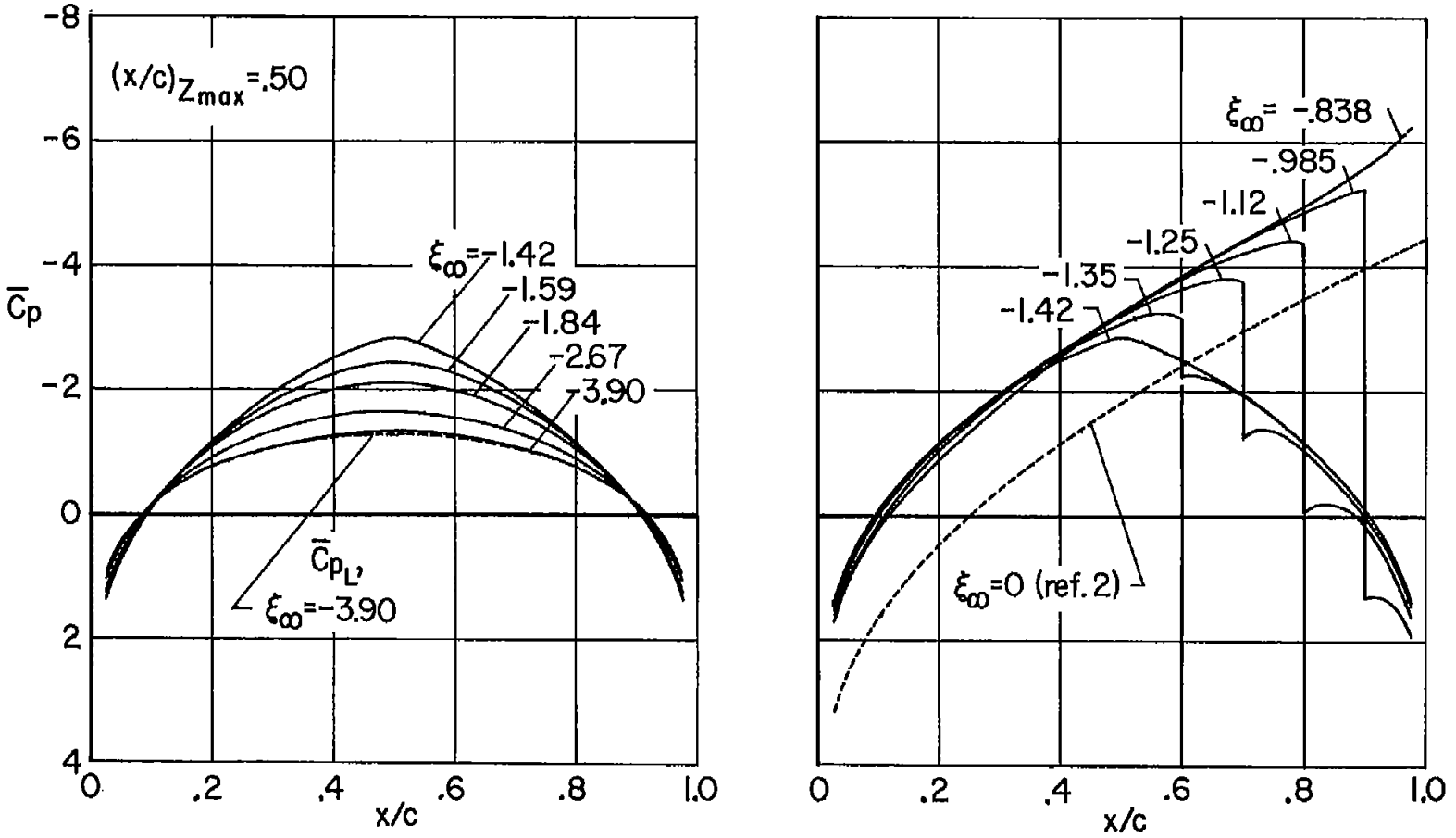

(a) $\xi_\infty \leq \xi_{\infty_{cr}}$

(b) $\xi_\infty \geq \xi_{\infty_{cr}}$

Figure 3.- Theoretical pressure distributions on an airfoil with maximum thickness at 50-percent chord.

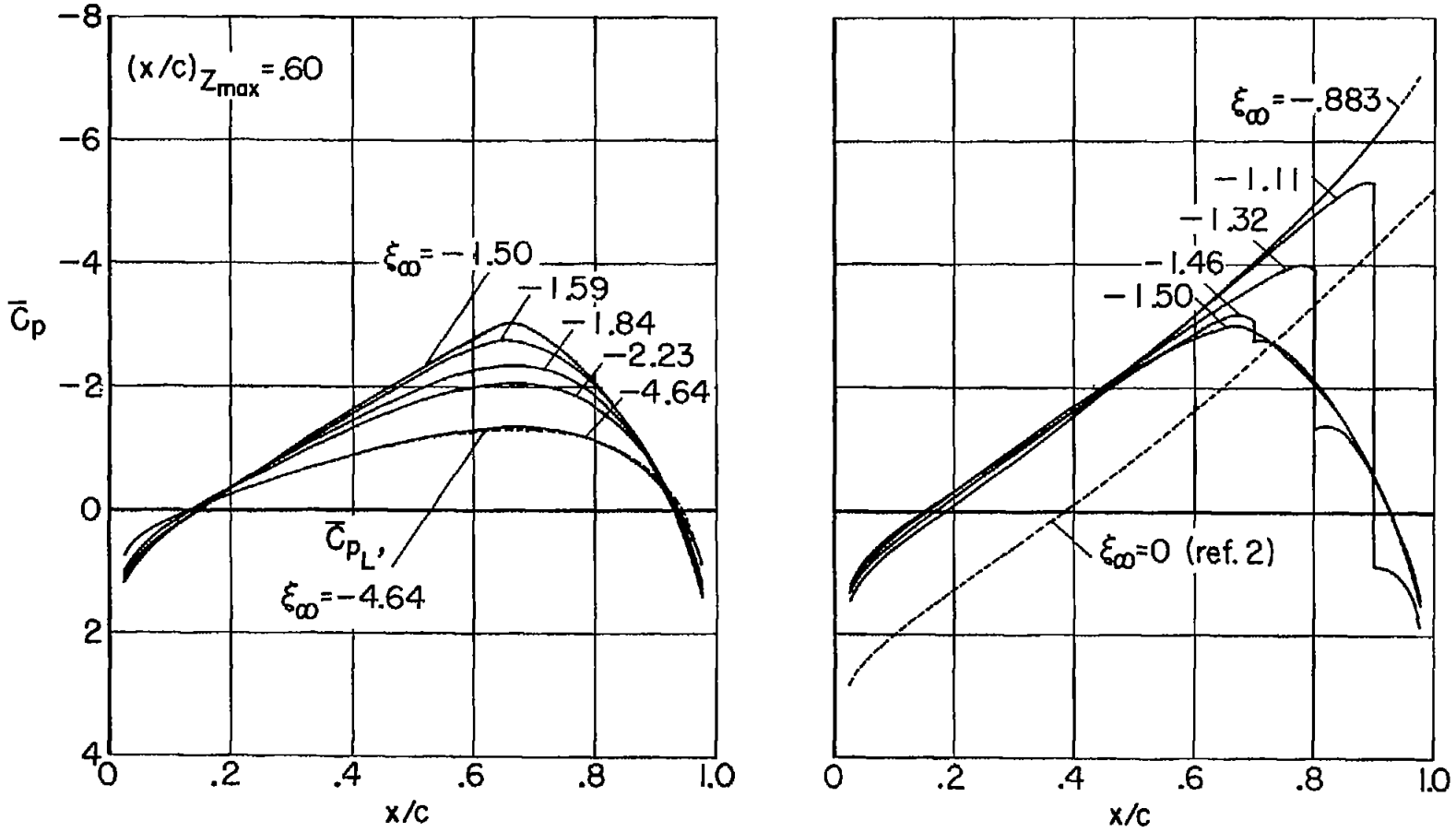

(a) $\xi_\infty \leq \xi_{\infty_{cr}}$

(b) $\xi_\infty \geq \xi_{\infty_{cr}}$

Figure 4.- Theoretical pressure distributions on an airfoil with maximum thickness at 60-percent chord.

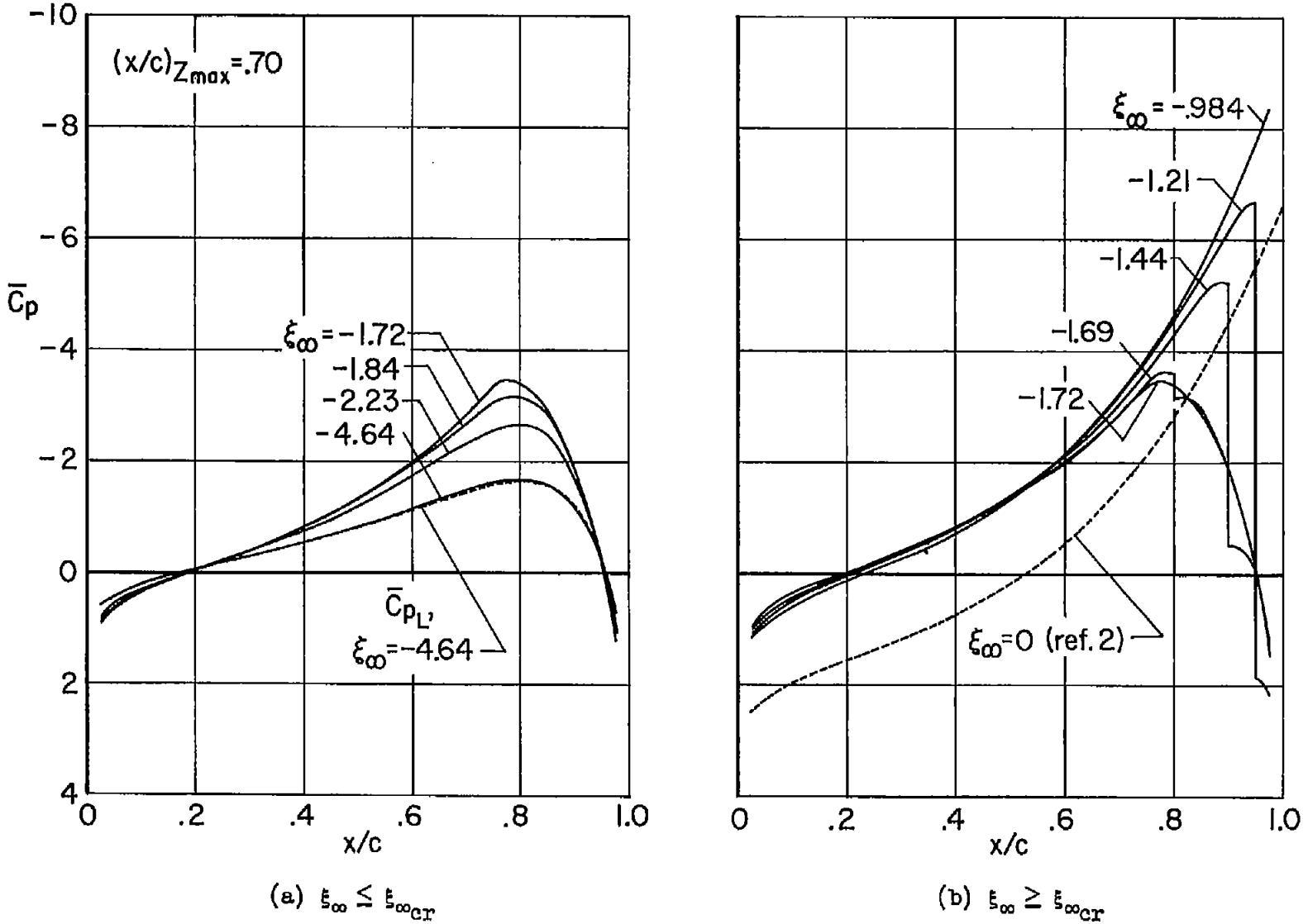

Figure 5.- Theoretical pressure distributions on an airfoil with maximum thickness at 70-percent chord.

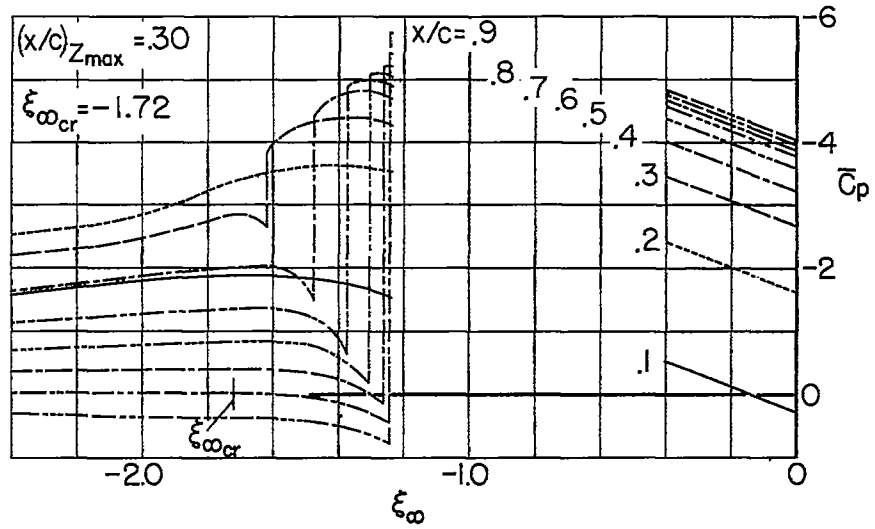

Figure 6.- Variation of reduced pressure coefficient $\bar{C}_p$ with Mach number parameter ξ_∞ for an airfoil with maximum thickness at 30-percent chord.

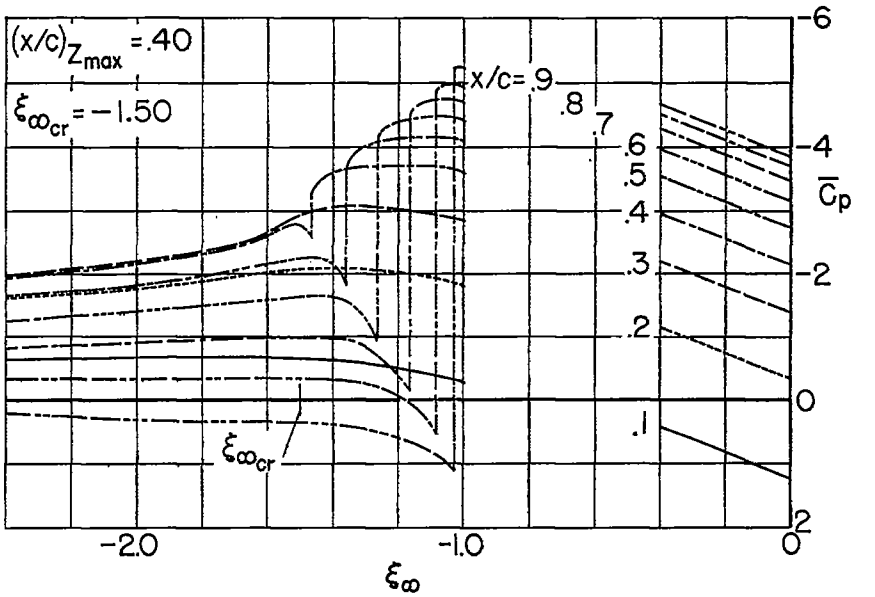

Figure 7.- Variation of reduced pressure coefficient $\bar{C}_p$ with Mach number parameter ξ_∞ for an airfoil with maximum thickness at 40-percent chord.

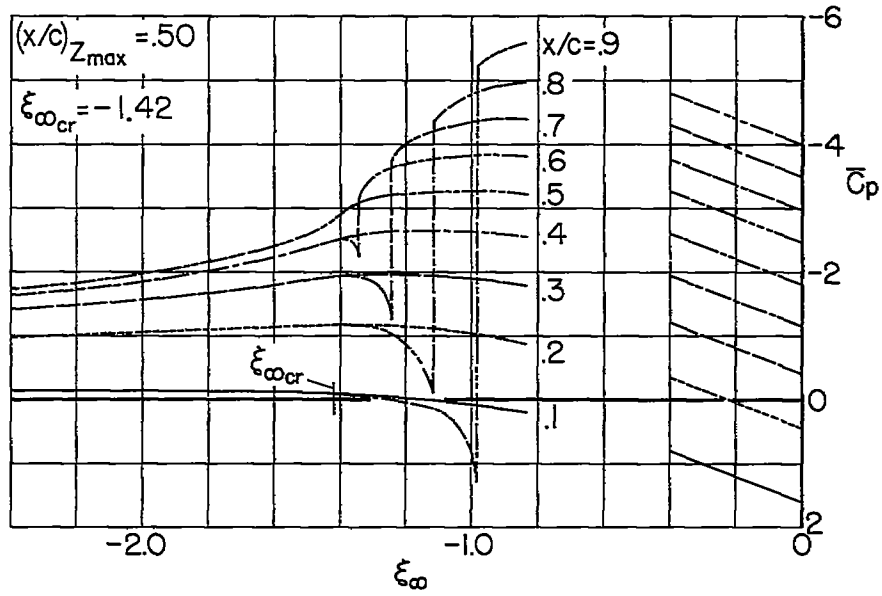

Figure 8.- Variation of reduced pressure coefficient $\bar{C}_p$ with Mach number parameter ξ_∞ for an airfoil with maximum thickness at 50-percent chord.

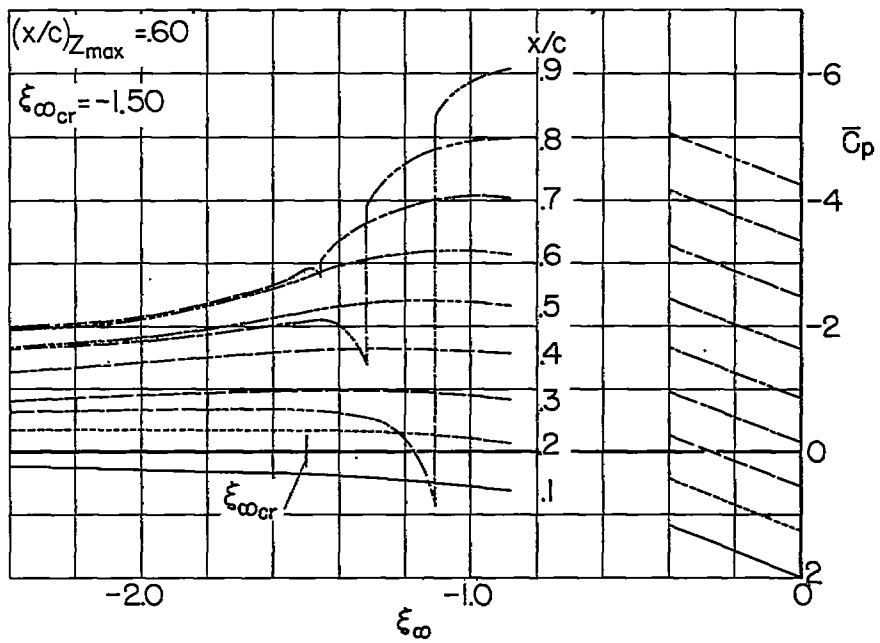

Figure 9.- Variation of reduced pressure coefficient $\bar{C}_p$ with Mach number parameter ξ_∞ for an airfoil with maximum thickness at 60-percent chord.

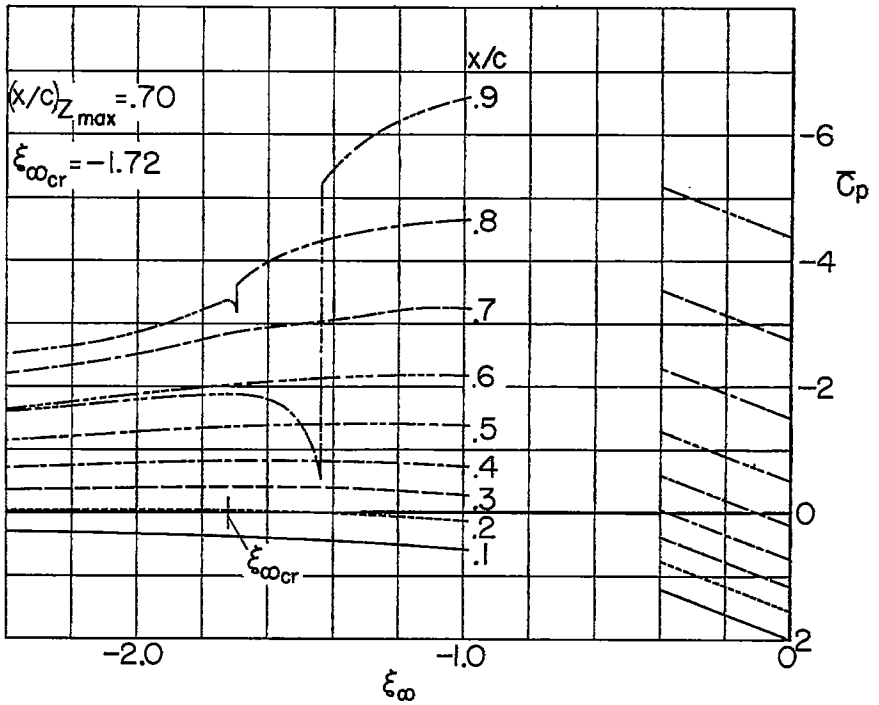

Figure 10.- Variation of reduced pressure coefficient $\bar{C}_p$ with Mach number parameter ξ_∞ for an airfoil with maximum thickness at 70-percent chord.

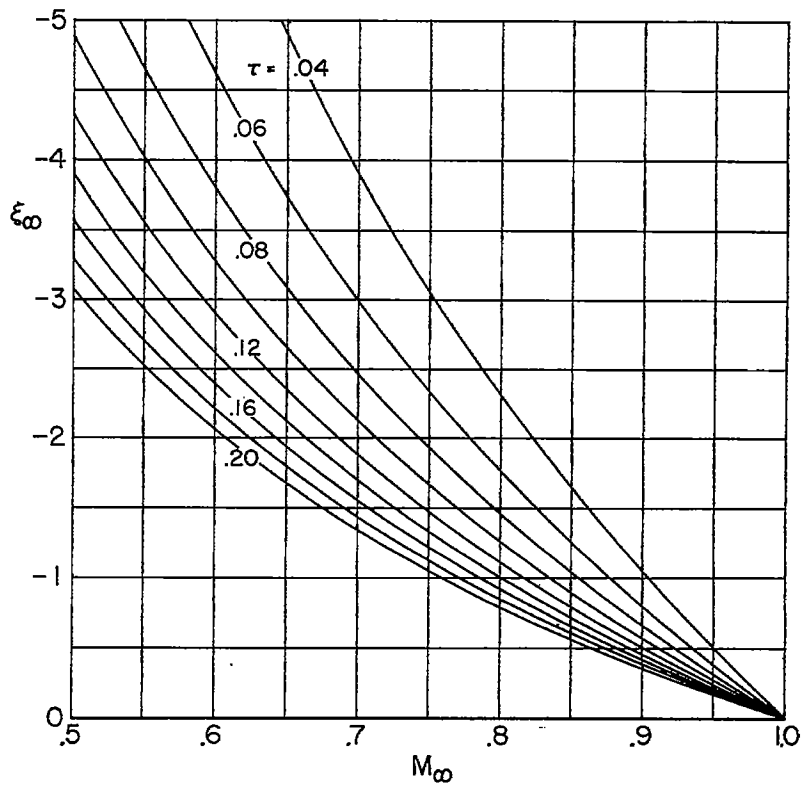

Figure 11.- Variation of Mach number with Mach number parameter ξ_∞ for various values of thickness ratio τ.